Journal of Petroleum Science and Engineering 205 (2021) 108843

Contents lists available at ScienceDirect

Journal of Petroleum Science and Engineering

journal homepage: www.elsevier.com/locate/petrol

Chlorite authigenesis and its impact on reservoir quality in tight sandstone reservoirs of the Triassic Yanchang formation, southwestern Ordos basin, China

Ke Li [a], Kelai Xi [a,b,*], Yingchang Cao [a], Xiaobing Niu [c], Songtao Wu [d], Shengbin Feng [c], Yuan You [c]

[a] Shandong Provincial Key Laboratory of Deep Oil and Gas, China University of Petroleum, Qingdao, Shandong, 266580, China
[b] State Key Laboratory of Continental Dynamics, Northwest University, Xi'an, 710069, China
[c] PetroChina Changqing Oilfield Company, Xi'an, 710065, China
[d] Research Institute of Petroleum Exploration & Development, Beijing, 100083, China

ARTICLE INFO

Keywords:
Authigenic chlorite
Reservoir quality
Tight sandstones
Yangchang formation
Ordos basin

ABSTRACT

Authigenic chlorite plays an important controlling role in reservoir quality, and is widely distributed in the tight sandstone reservoirs of the Triassic Yanchang Formation in the Southwestern Ordos Basin, China. The occurrence and origins of authigenic chlorite were investigated using an integrated approach of optical microscopy, scanning electron microscopy, X-ray diffraction, electron probe microanalysis, and fluid inclusion analysis. The sandstones are fine-grained lithic arkoses and feldspathic litharenite with 11.5% volcanic rock fragments. Authigenic chlorite occurs in two morphotypes, including pore-lining and pore-filling chlorite. Pore-lining chlorite occurs as coatings on the framework grains and covers the entire fining-upward sandstones. Pore-filling chlorite is restricted to the middle to upper part of the fining-upward sandstones and appears as discrete flaky plates or rosettes in the pores or attaches to the surfaces of pore-lining chlorite. Pore-lining chlorite originated from smectite precursors that were derived from volcanic material alteration in the early stage of diagenesis, with temperatures primarily about 90 °C. In contrast, pore-filling chlorite was precipitated in pore spaces with higher concentrations of Mg^{2+} and Fe^{2+} released from volcanic rock fragments and mica debris dissolution. Moreover, the chemical composition of pore-filling chlorite was affected by early calcite cementation which consumed some ions at temperatures lower than about 110 °C. The thin and continuous pore-lining chlorite is the only chlorite type with a positive effect on reservoir quality, whereas the very thick pore-lining chlorite (>6.7 μm) or pore-filling chlorite significantly reduce the porosity and permeability. Systematic studies of authigenic chlorite can provide important insights into the reservoir heterogeneity and are applicable to the exploration and development of tight oil.

1. Introduction

Reservoir quality plays a key role in the efficient exploration of tight sandstone oil resources (Zhou et al., 2016; Wang G. et al., 2017). Diagenetic modifications are the most significant process controlling reservoir quality and may produce a strong petrophysical heterogeneity in tight sandstone reservoirs (Fitch et al., 2015; Li Z. et al., 2017a, 2017b; Xi et al., 2019a, 2019b; Jafari et al., 2020). Generally, tight sandstone reservoirs have undergone complex diagenetic alterations (Karim et al., 2010; Dutton and Loucks, 2010; Wolela, 2012), forming several kinds of authigenic minerals in intergranular pores and as overgrowths on detrital particles (Luo et al., 2014; Lai et al., 2015). Those like carbonates and zeolites that form cements, as well as quartz overgrowths are the main factors adversely impacting reservoir quality (Zhang et al., 2012; Mao et al., 2019; Li et al., 2020). However, authigenic clay minerals, especially chlorite, may induce both positive and negative implications on the reservoir quality (Billault et al., 2003; Yao et al., 2011; Huggett et al., 2015; Ma et al., 2017a; Zhu et al., 2017; Cao et al., 2018; Zhou X. et al., 2018a, 2018b). For example, kaolinite and illite are usually detrimental to reservoir quality, but chlorite fillings may preserve reservoir properties, depending on their occurrence modes (Bahlis and Ros, 2013; Wang M. et al., 2017). Large quantities of chlorite were always found in reservoirs with abnormally high porosity (Ehrenberg, 1993; Anjos et al., 2003). Consequently, chlorite

* Corresponding author. Shandong Provincial Key Laboratory of Deep Oil and Gas, China University of Petroleum, Qingdao, Shandong, 266580, China.
E-mail address: xikelai@upc.edu.cn (K. Xi).

https://doi.org/10.1016/j.petrol.2021.108843
Received 4 June 2020; Received in revised form 29 March 2021; Accepted 17 April 2021
Available online 22 April 2021

authigenesis has attracted particular attention due to the combination of positive and negative implications for reservoir quality (Huang et al., 2004; Berger et al., 2009).

Previous studies have concluded that pore-lining and pore-filling chlorite are the two main types in many tight sandstone reservoirs (Grigsby, 2001; Cao et al., 2018). The impact of pore-filling chlorite on reservoir quality is generally considered negative, but the impact of pore-lining chlorite on reservoir quality is still controversial (Berger et al., 2009; Zhang et al., 2012; Zhou et al., 2017; Worden et al., 2020). The reason is likely an ambiguous understanding of the genesis of the mechanism of chlorite in the reservoirs. The formation of chlorite in sandstone reservoirs can be roughly categorized into three types: the transformation of clay mineral precursors, the transformation of mafic rocks, and precipitation from pore water (Anjos et al., 2003; Zhang et al., 2012; Haile et al., 2015; Zhu et al., 2017). Chlorite crystals produced by different diagenetic processes have different growth habits (Ehrenberg, 1993; Berger et al., 2009; Zhou et al., 2017). Moreover, different types of chlorite may have originated from various processes at different diagenetic stages (Grigsby, 2001; Yao et al., 2011; Ma et al., 2017b). These differences have a significant influence on other diagenetic processes and eventually affect the reservoir quality of sandstones. For example, early-formed pore-lining chlorite can prevent compaction and quartz overgrowth (Ehrenberg, 1993; Gould et al., 2010), but late-formed chlorite destroys the pore spaces, regardless of whether it is pore-lining or pore-filling chlorite (Ma et al., 2017b; Zhou X. et al., 2018). Thus, an in-depth study of the genesis of authigenic chlorite is crucial to understand the heterogeneity of tight sandstone reservoirs.

The Ordos Basin is an important petroliferous basin in China, and the Triassic Yanchang Formation is its main reservoir. Authigenic chlorite was extensively found in these reservoirs (Zhang et al., 2012; Zhu et al., 2017), and it has been demonstrated that chlorite is one of the primary controlling elements of reservoir heterogeneity (Xi et al., 2019a; Li et al., 2020). To date, some works mainly analyzed the occurrence modes of authigenic chlorite (Zhang et al., 2012; Zhou et al., 2017), but the formation mechanisms of different types of chlorite have not been sufficiently investigated (Xiang et al., 2016; Fan et al., 2017; Zhou et al., 2017). In addition, there are few detailed discussions on the authigenic chlorite under a sandstone sequence. Therefore, determining the occurrence, distribution characteristics, formation period and genesis of chlorite is of great significance for predicting the reservoir heterogeneity. The objectives of this study are to (1) perform a detailed investigation of the types and distribution patterns of authigenic chlorite in the Yanchang Formation, (2) clarify the origins of authigenic chlorite, and (3) determine the impact of authigenic chlorite on reservoir heterogeneity.

2. Geological background

As a multicyclic petroliferous basin, the Ordos Basin developed in the west of the North China platform (Fig. 1A). The basin is encircled by five mountain ranges, i.e., the Yinshan Mountains (Mts) in the north, the Qinling Mts in the south, the Helan Mts and the Liupan Mts in the west, and the Luliang Mts in the east (Fig. 1A). The Ordos Basin covers approximately 250,000 km^2, second only to the Tarim Basin in China. The Ordos basin has a gentle monoclinal structure that is higher in the east and lower in the west, with a dip angle of below than 1° (Lai et al., 2016). The basin can be subdivided into 6 first-order sub-tectonic units of the Yimeng uplift, the Shanbei slope, the Tianhuan depression, the western edge thrusting belt, the Jinxi fold belt, and the Weibei uplift (Fig. 1A). This paper focuses on the southwest of the basin, which is one of the most developed areas in the Triassic oil and gas reservoir, including the Jiyuan, Huanjiang, and Longdong areas (Fig. 1A).

The tectonic framework of the Ordos Basin was formed mainly in the Mesozoic (Zhao et al., 2012). During that time, the basin was affected by the three major tectonic domains of the Paleo-Tethys Ocean, the Pacific Rim, and the Paleo-Asian Ocean. Intense tectonic activities around the basin resulted in the formation of the Luliang Uplift, the Yinshan Magmatic Belt, and the Liupanshan Thrust Belt. Influenced by the Yanshanian Orogeny (Early Jurassic- Late Cretaceous) in the later period of tectonic evolution, the eastern part of the basin continued to uplift, forming the east-west structural feature that currently exists (Zhao et al., 2012). The Yanchang Formation experienced a whole evolutionary cycle of the inland lake basin, including the formation, expansion, intense depression, gradual shrinkage, and extinction of the lake, forming a sedimentary system type dominated by alluvial fans, a fan delta, and lacustrine deposits (Zhu et al., 2013). The thickness of the Yanchang Formation is in a range of 200 m–1400 m, and the sediments can be subdivided into Chang 1 to Chang 10 from shallow to deep, representing 10 oil-rich members (Fig. 1B). The paleo–Ordos lake expanded in Chang 10-Chang 7, shrank in Chang 6-Chang 4, and disappeared in Chang 3-Chang 1 (Guo et al., 2018). The Chang 7 and Chang 4 + 5 members are mainly deep lacustrine and shallow lacustrine deposits, respectively, and the lithology consists of mainly dark shales, which are good source rocks (Yang et al., 2013; Zhu et al., 2013; Ju et al., 2020). The study

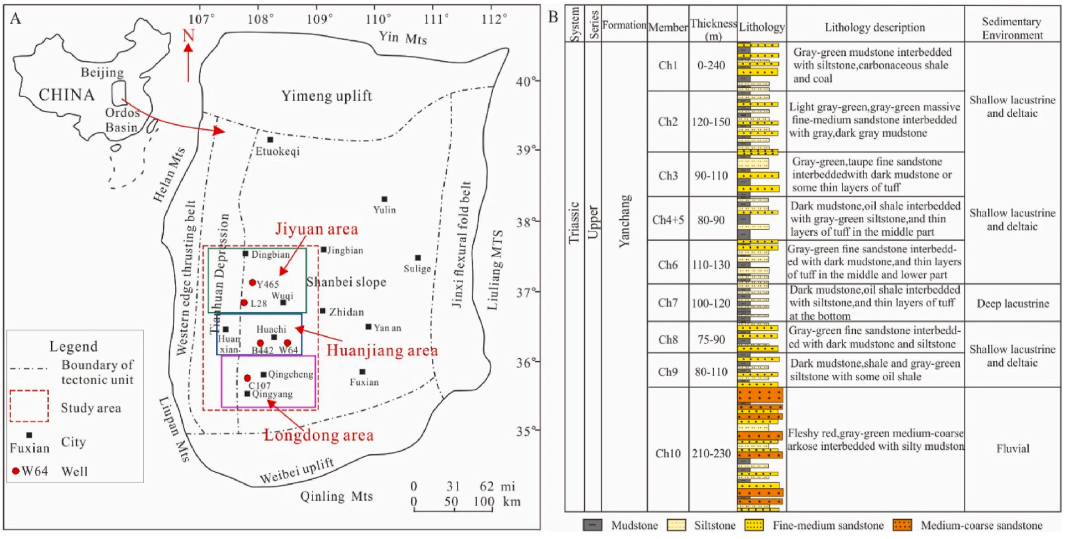

Fig. 1. Location map and subtectonic units of the Ordos Basin and the Yanchang Formation stratigraphy. (A) Location and subtectonic units of the Ordos Basin. (B) Generalized Upper Triassic Yanchang Formation stratigraphy of the Ordos Basin. Ch-Chang (modified from Hu et al., 2018).

members Chang 8 and Chang 9 were mainly deposited in shallow lacustrine and deltaic sediments (Wang G. et al., 2017). Moreover, the Chang 9 member contains a small quantity of shale that forms not only reservoirs but also source rocks (Yao et al., 2018).

3. Data and methods

Over 500 core samples and about 5500 reservoir porosity and permeability data were obtained from the Research Institute of Petroleum Exploration and Development, Changqing Oilfield Company, PetroChina. About 200 casting thin sections were prepared for the study of diagenetic chlorite. The thin sections were stained with Alizarin red to facilitate the visual detection of different carbonate minerals. The analysis of the thin sections was performed using point-counting methods (400 points per sample) to determine the composition characteristics. A Zeiss Axioscope A1 APOL digital transmission microscope with Image-Pro Plus software was used to evaluate sandstone sorting and measure the particle size of the samples. The whole rock (bulk) and clay fraction (<2 μm) mineralogy of 246 sandstone samples were analyzed by X-ray diffraction (XRD). In addition, the methods described by Moore and Reynolds (1999) and Hillier (2003) were used for sample preparation, analysis, and interpretation.

A total of 22 chlorite-rich rock samples and 18 thin sections were analyzed using a scanning electron microscope (SEM) coupled with an energy-dispersive spectrometer (EDS) to detect and characterize the minerals and determine the petrographic relationships. The samples were Pt-coated and observed under an SEM (Quanta FEG 450) at 20 keV.

MAPS mineralogy analysis of high-resolution backscattered electron (BSE) images was used to characterize the authigenic minerals. According to the thin section analysis, 5 rock samples were chosen for MAPS mineralogy analysis using an FEI Helios 460 instrument equipped with an EDS. These samples contained different chlorite contents and were representative of the lithological characteristics of the study area. The samples were polished and were analyzed with the EDS probe. The scanning resolution was 20 nm with an acceleration voltage of 3 keV and a beam current of 0.4 nA. The BSE images were collected and mosaicked into high-resolution images. The quantitative evaluation of the minerals was performed using the QEMSCAN analysis. In each sample, we scanned 9 fields to create nine grids, which required about 3 h.

A total of 13 chlorite-rich thin sections located in different positions of the lithofacies association were chosen from representative wells for the electron probe microanalysis (EPMA) and BSE image microanalysis using a JXA-8230 instrument (JEOL) at an accelerating voltage of 20 keV and a beam current of 10 nA with a beam diameter <1 μm. The thin-section samples were coated with carbon. The chlorite in the pores and chlorite coatings were analyzed. Data with a total oxide content greater than 65% were selected, and those with ($NaO + K_2O + CaO$) < 0.5% were eliminated to reduce mixed dye (Foster, 1962).

Six double-polished thin sections were chosen for fluid inclusion petrographic analyses and microthermometric measurements using a calibrated Linkam THMSG 600 heating and cooling stage. The homogenization temperature (Th) was determined using a heating and cooling rate of 10 °C/min at temperatures of 0–60 °C or below−20 °C, and 5 °C/min at temperatures of -20-0 °C or higher than 60 °C. The measurement precision was ±1 °C for the Th and ±0.1 °C for the final ice melting temperature.

The thin section and fluid inclusion analyses were performed in the Reservoir Geology and Basin Analysis Key Laboratory of the China University of Petroleum. The XRD and SEM analyses and the quantitative evaluation of the minerals using SEM (QEMSCAN) and MAPS mineralogy were conducted in the Key Laboratory of Oil and Gas Reservoir of PetroChina. The BSE and EPMA analyses were performed in the Key Lab of Submarine Geosciences and Prospecting at the Ocean University of China.

4. Results

4.1. Sandstone petrography

The tight sandstones of the Chang 8 and Chang 9 Members are primarily lithic arkose and feldspathic litharenite, with an average framework composition of $Q_{36}F_{40}L_{24}$ (Fig. 2A). Detrital quartz comprises 24–53%, with an average of 35.9%; feldspar grains account for 21–45%, with an average of 40.1%. Rock fragments comprise 5–32%, with an average of 24%. The rock fragments are mostly volcanic fragments (11.5%) and low-grade metamorphic fragments (8.5%), with few sedimentary fragments (2.0%) (Fig. 2B and C). The volcanic rock fragments (VRFs) includes andesite clasts, basalt clasts, and tuff clasts. The metamorphic rock fragments include phyllites, slates, quartz mica schist, and metamorphic quartzite. In addition, a few sedimentary rock clasts, such as mudstone clasts and some bio-detritus, are also observed. Moreover, the porosity obtained from point counting comprises 0.4–16.5%, with an average of 9.8%. The tight sandstones are mainly fine-grained and well sorted. The sandstones have a mature texture, but the composition is immature.

XRD analyses indicate that chlorite is the dominant clay mineral, accounting for about 65% of total clay minerals and ranging from 15% to 95%. Mixed-layer illite/smectite (I/S), illite, and kaolinite are also found in some wells but with low content. Smectite is not present in most of the samples. Chlorite extensively occurs in the intergranular pores, showing both pore-lining and pore-filling characteristics (Fig. 2D).

4.2. Diagenetic minerals

4.2.1. Calcite and quartz cement

Calcite cement is the main cement type in the sandstone of the upper Triassic Yanchang formation, with an average content of 3.6%. After dyeing with alizarin red, calcite appears purple-red, with pore-filling blocky or patchy aggregates (Fig. 3A–D). Notably, two calcites with different characteristics are observed in the sandstones. The first one is present as a patch aggregates in the pores attached to the chlorite coatings (Fig. 3A). However, the other one completely fills the pores, and there is no chlorite at the contact edge with the grains (Fig. 3B). In the high-resolution photomicrograph of MAPS, the first type of calcite cementation seems to inhibit the growth of chlorite (Fig. 3C).

Quartz cements are another common cement in the investigated tight sandstone reservoirs, and the average content is 0.58%. Generally, quartz cements are characterized by authigenic quartz particles in the pores and few quartz overgrowths (Fig. 3D and E). Quartz overgrowths are not common in the study area and often develop in locations where chlorite coats are discontinuous or undeveloped (Fig. 3D). Moreover, it is observed that quartz overgrowths are surrounded by calcite in some cases (Fig. 3D). Authigenic quartz commonly develops in reservoirs with abundant feldspar dissolution pores. In some samples, authigenic quartz grains are replaced by irregular flaky plates of chlorite (Fig. 3F).

4.2.2. Authigenic chlorite

4.2.2.1. Morphology of chlorite. Two different morphologies of chlorite have been identified in the tight sandstone reservoirs of the Triassic Yanchang Formation. The first type of chlorite mainly occurs as pore-lining coatings on detrital grains, growing perpendicular from the grain to the intergranular pores (Fig. 4A). The other type of chlorite appears as pore-filling clays in intergranular pores or is attached to the surfaces of chlorite coatings (Fig. 4B). The pore-lining chlorite coatings occurs as poor flaky plate crystals, with a thickness of about 3–10 μm (Fig. 4C and D). The pore-filling chlorite occurs in discrete flaky plates or rosette-shaped crystalline aggregates, and the size of most aggregates is larger than 8 μm (Fig. 4B, E-F). In the high-resolution photomicrograph of MAPS, a boundary layer occurs between the two types of chlorite,

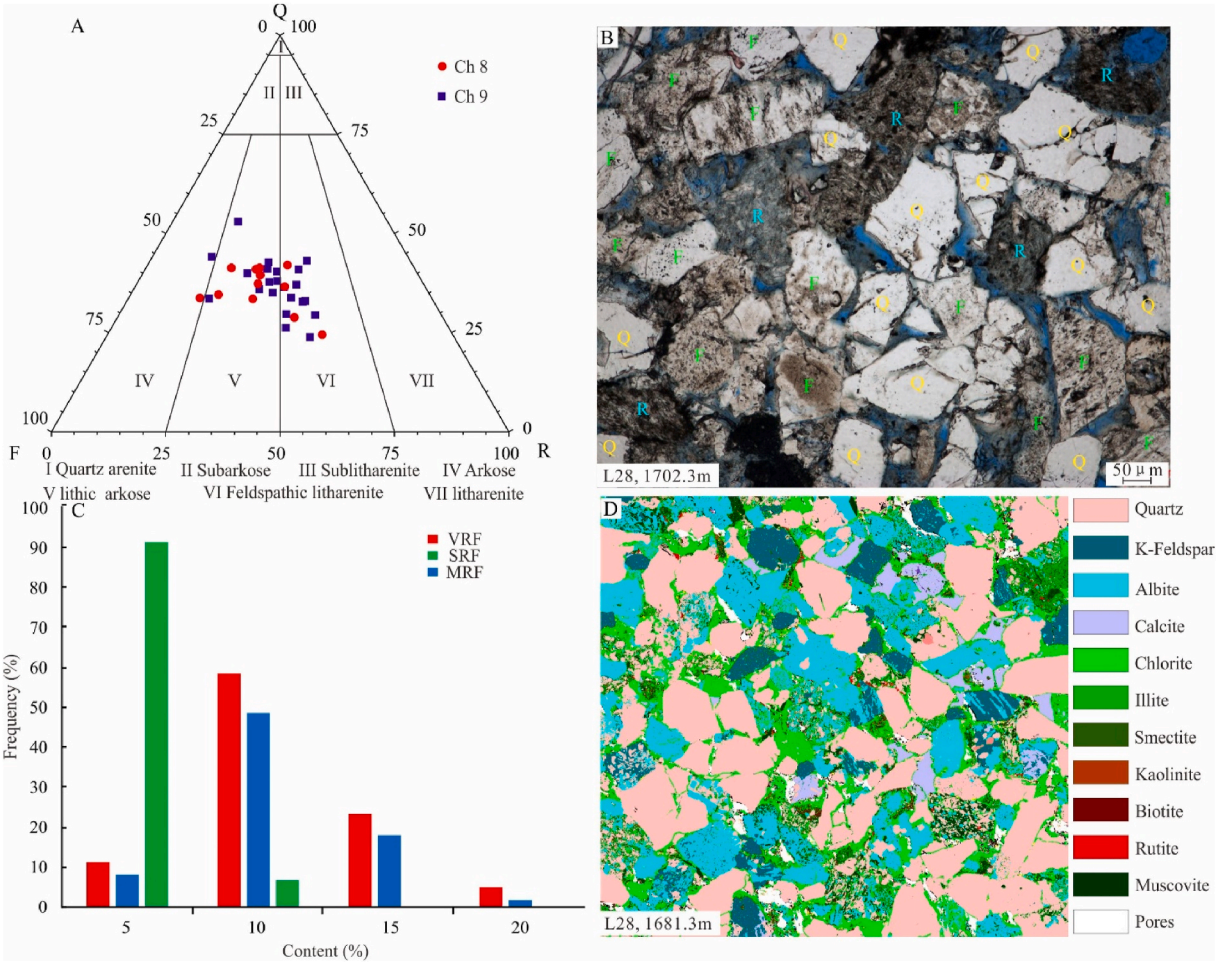

Fig. 2. Rock compositions of the tight sandstone reservoirs in the Upper Triassic Yanchang Formation. (A) Classification of sandstone based on Folk's (1974) criteria. (B) Photomicrograph of thin sections under plane-polarized light showing textural characteristics of the sandstones. (C) Composition characteristics of the sandstones. VRF = volcanic rock fragments SRF = sedimentary rock fragments MRF = Metamorphic rock fragments. (D) Classification of the mineral composition in the scanning electron microscope photomicrographs in the L28 sample (1681.3 m).

showing an inner layer with a tight rim and scattered euhedral crystals on the outside (Fig. 4F–H). Calcite has developed on top of the pore-lining chlorite coatings in intergranular pores of some samples (Fig. 4I).

4.2.2.2. Distribution of chlorite. The thin section analyses show that chlorite cements are distributed heterogeneously in the tight sandstone reservoirs. The content of chlorite is significantly affected by the grain size distribution of the tight sandstones. Chlorite is concentrated in the sandstones, with a particle size of 0.2–0.4 mm (Fig. 5). The content of chlorite is considerably lower when the grain size is smaller than 0.2 mm or larger than 0.5 mm (Fig. 5).

The Chang 8 and Chang 9 members were mainly deposited in the braided-delta subaqueous distributary channels, and the sediments with different grain sizes are vertically combined into three patterns, namely, the fining-upward sandstones, sandstone-mudstone interbedding units, and coarsening-upward sandstones. Chlorite develops primarily in the fining-upward sandstones, showing heterogeneous distribution in sandstones. The content of chlorite ranges from 5.4 to 22.0% (Fig. 6). In general, the content of chlorite is lower in the bottom part than the middle and upper part of the fining-upward sandstones, which opposite to the content of calcite cements (Fig. 6). The strong volcanic fragments dissolution is also in the middle to upper part of the fining-upward sandstones with higher chlorite content, especially the pore-filling chlorite (Fig. 6). However, in the bottom of the sandstones with lower chlorite content, pore-lining chlorite is more common, and pore-filling chlorite is rarely observed (Fig. 6). In these reservoirs, the pores are mainly filled with calcite, the pore-filling chlorite rarely develops, and the pore-lining chlorite is very thin (Fig. 6). In other words, pore-lining chlorite is widely distributed in the fining-upward sandstones, whereas pore-filling chlorite primarily develops in the middle to upper part of the sandstones.

4.2.2.3. Chemistry of chlorite. Although the total amount of oxides obtained from the EPMA is less than the theoretical value (85%–88%) due to the high micro-pores and water content in the chlorite, these results do not affect the analysis of the chlorite structure (Hillier, 1994; Berger et al., 2009; Zhang et al., 2012; Ma et al., 2017b). The results show that chlorite consists primarily of Al_2O_3, FeO, SiO_2, and MgO (Table 1). The content of Al_2O_3 in the chlorite ranges from 14.1% to 21.6%, with an average of 17.9%; SiO_2 ranges from 17.0% to 27.5%, with an average of 23.1%; FeO is between 16.1% and 28.9%, with an average of 22.5%; MgO ranges from 5.6% to 11.1%, with an average of 8.54%. In addition, chlorite also contains a small amount of Na_2O (0.1%), K_2O (0.06%), CaO (0.16%), and MnO (0.34%), and some impurities, such as TiO_2 (0.02%) and Cr_2O_3 (0.03%). The structure of chlorite was determined using the data on the basis of 28 oxygen equivalents (Table 2). Since the data of Fe_2O_3 were not obtained by EPMA, all Fe irons were assumed to be Fe^{2+}. The EPMA analyses reveal that the chlorites of the Yanchang formation are relatively rich in iron, and the ratios of Fe/Fe + Mg are in the range of 0.54–0.68, with an average of 0.60. The two types of chlorite cements appear to have

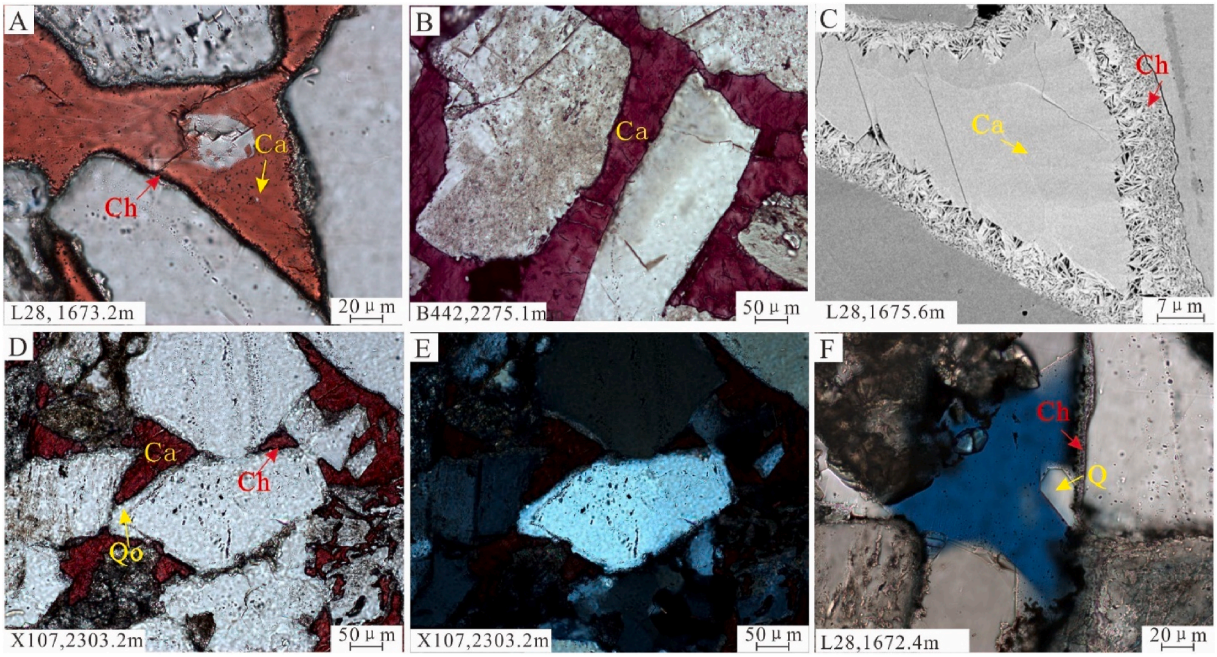

Fig. 3. Types and characteristics of diagenetic minerals in the Upper Triassic Yanchang Formation. (A) Photomicrograph of thin sections under plane-polarized light showing calcite (Ca) with chlorites (Ch) in the L28 sample (1673.2 m). (B) Microphotograph under plane-polarized light showing calcite (Ca) without chlorites in the B442 sample (2275.1 m). (C)A MAPS mineralogy image showing calcite (Ca) with chlorites in the L28 sample (1675.6 m); calcite cementation seems to inhibit the growth of chlorites. (D) Microphotograph under plane-polarized light showing quartz overgrowth (Qo) in the X107 sample (2303.2 m). (E) Microphotograph under orthogonal light showing quartz overgrowth in the X107 sample (2303.2 m). (F) Microphotograph under plane-polarized light showing quartz cement in the pores of the L28 sample (1675.3 m).

distinct elemental compositions. The average formula of the pore-lining chlorite is $(Al_{1.77}Fe_{2.31}Mg_{1.46}Mn_{0.03}Ca_{0.03}K_{0.03}Na_{0.06})_{5.69}[(Si_{2.96}Al_{1.04})_4O_{10}](OH)_8$ and that of the pore-filling chlorite is $(Al_{1.55}Fe_{2.43}Mg_{1.71}Mn_{0.04}Ca_{0.02}K_{0.01}Na_{0.05})_{5.66}[(Si_{2.82}Al_{1.08})_4O_{10}](OH)_8$ (Table 2). The pore-filling chlorite contains more abundant Mg ions, whereas the pore-lining chlorite has a higher Al content (Fig. 7). The Fe/Fe + Mg ratio of the pore-lining chlorite ranges from 0.59 to 0.68, with an average of 0.61, which is higher than that of the pore-filling chlorite, which has a range of 0.54–0.64 and an average of 0.59 (Table 2). The Na and K content is higher in the pore-lining chlorite, and the Mn content is slightly higher in the pore-filling chlorite (Fig. 7).

4.3. Fluid inclusion

Fluid inclusions commonly exist in calcite cements and quartz cements. Most of the fluid inclusions consist of two phases, gas and liquid, at room temperature. The Th of the calcite cements without chlorite (Ca–I) is 81.8–96.7 °C, and the average is 90.2 °C, whereas that of the calcite cements with chlorite coatings (Ca-II) ranges from 97.6 °C to 111.8 °C, with an average of 107 °C (Table 3). The data of the fluid inclusions reveals that the quartz overgrowths (Qo-I) precipitated at temperatures ranging from 89.3 °C to 108 °C, with an average of 97.0 °C, whereas the authigenic quartz grains (Qo-II) formed at higher temperatures ranging from 119.2 °C to 122.2 °C, with an average of 120.8 °C (Table 3).

5. Discussion

5.1. Paragenetic sequence of diagenetic minerals

Chlorite paragenesis was preliminarily determined by the textural relationships. First, pore-lining chlorite is not observed in the reservoirs where the grains are in close contact, demonstrating that the pore-lining chlorite was formed after initial compaction. Second, there is no chlorite in the pores filled by the Ca–I (Fig. 3B), whereas the Ca-II fills the pores with pore-lining chlorite (Fig. 3A). This result indicates that pore-lining chlorite occurred later than the Ca–I deposition and earlier than the Ca-II formation. In addition, Qo-I only occurs in places where the pore-lining chlorite was discontinuous or undeveloped, indicating that pore-lining chlorite formed earlier than the Qo-I (Fig. 3D). Lastly, pore-filling chlorite does not occur where Ca-II filled the pores since the growth of pore-filling chlorite is restricted by Ca-II ((Figs. 3B and 6). As a result, the pore-filling chlorite cemented later than the later calcite (Ca-II). Based on the results of the fluid inclusions, the formation temperature of Ca–I is about 90.2 °C, which is lower than that of Ca-II (about 107 °C), indicating that Ca–I formed earlier than Ca-II (Fig. 8). In addition, the average formation temperature of Qo-I is 97.0 °C, indicating that it formed earlier than Qo-II, whose average formation temperature is 120.8 °C (Fig. 8). These analyses show that the diagenetic sequence of the study area is as follows: Initial compaction - first stage calcite (Ca–I) - pore-lining chlorite (Ch-1) – first-stage quartz cementation (Qo-I) – second-stage calcite (Ca-II) - pore-filling chlorite (Ch-2) or second stage authigenic quartz (Qo-II) (Fig. 9). Pore-lining chlorites formed at temperatures of about 90 °C, and pore-filling chlorites formed at temperatures of about 110 °C.

5.2. Development and origins of authigenic chlorite

The composition of chlorite is complex, and ion substitution often occurs due to environmental changes. The most important reaction is the substitution reaction between Al^{3+}, Si^{4+}, Mg^{2+}, Fe^{2+}, and Fe^{3+}. Al^{3+} can be substituted for Si^{4+} at the tetrahedral sites to form tetrahedral Al (Al^{IV}) and also for Mg^{2+}, Fe^{2+}, and Fe^{3+} at the octahedral sites to form octahedral Al (Al^{VI}) (Murray, 2007; Worden et al., 2020). In the pore-lining chlorite and the pore-filling chlorite, the content of Al^{VI} is more abundant than Al^{IV}, and the octahedral occupancy (Sum VI) is less than the ideal number (which is 12) (Fig. 10A and B). These characteristics are different from metamorphic chlorite (Foster, 1962) but similar to diagenetic chlorite (Hillier, 1994; Billault et al., 2003; Zhang et al., 2012; Ma et al., 2017b; Zhu et al., 2017). The pore-lining and

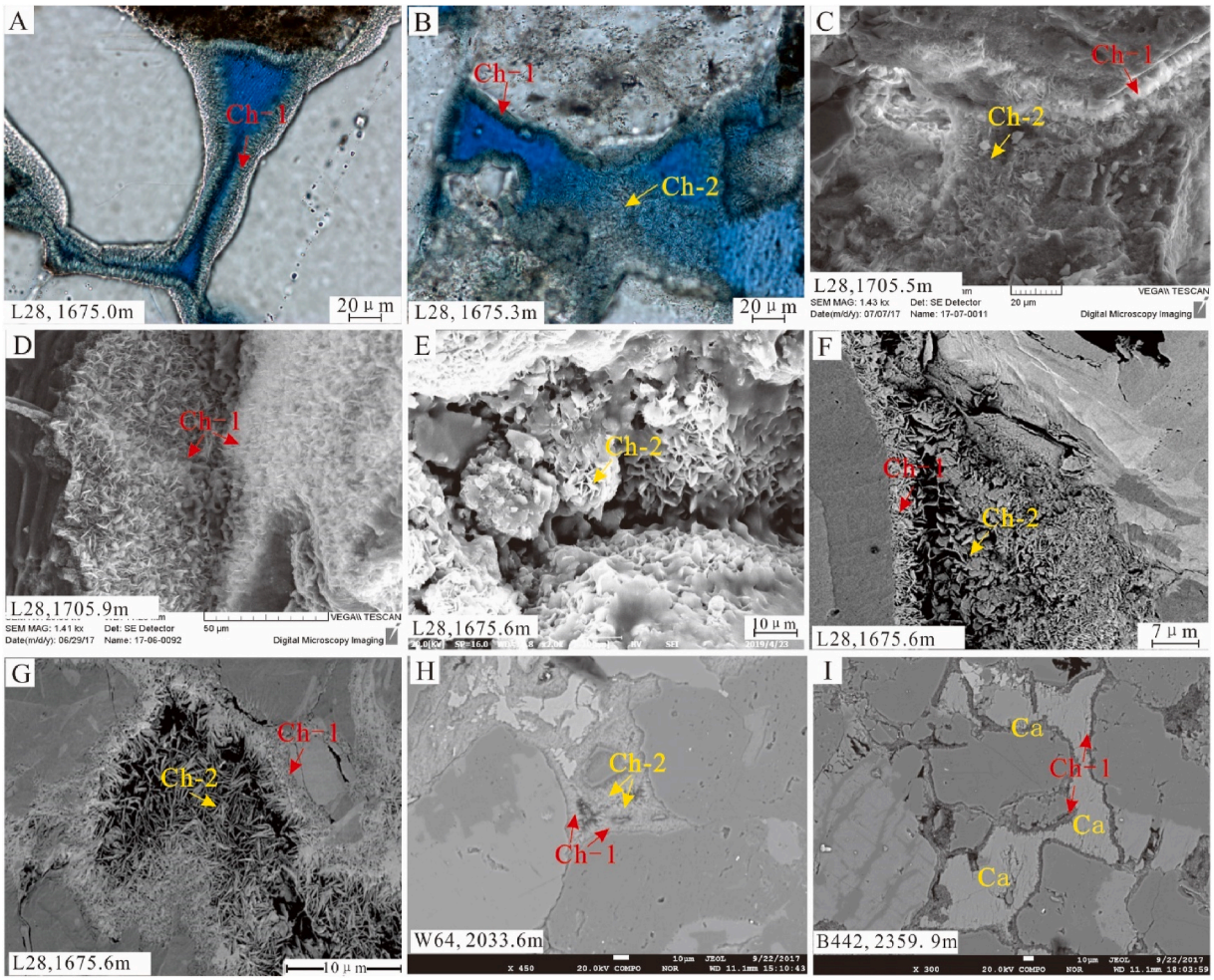

Fig. 4. Types and characteristics of the chlorite in the Upper Triassic Yanchang Formation. (A) Photomicrograph of thin section showing pore-lining chlorite (Ch-1) in the L28 sample (1675 m). (B) Photomicrograph of thin section showing pore-filling chlorite (Ch-2) in the L28 sample (1675.3 m). (C–E) Scanning electron microscope image showing the two types of chlorite in the L28 sample (1705.5 m, 1705.9 m, 1675.6 m). (F–H) Backscattered electron (BSE) image showing the two types of chlorite in the L28 sample (1675.6 m) and W64 sample (2033.6 m). (I) BSE image showing pore-lining chlorite (Ch-1) with calcite in the L28 sample (1671.92 m).

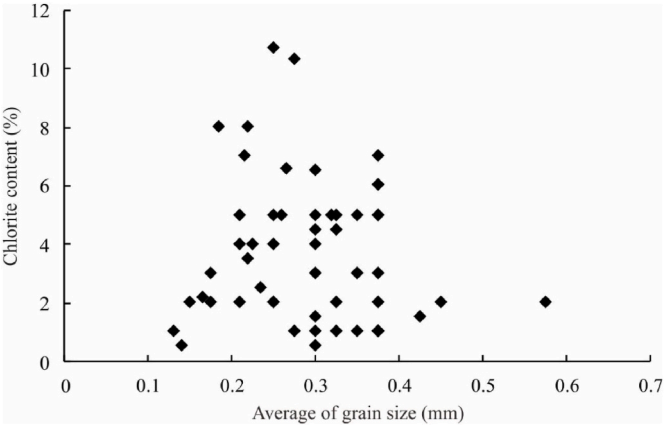

Fig. 5. The relationship between chlorite content and grain size in the Upper Triassic Yanchang Formation.

pore-filling chlorite are both typical diagenetic chlorite (brunsvigite) (Fig. 10C). Moreover, the pore-filling chlorite has higher contents of Sum VI and Al^{VI}, but the Si^{4+} content is lower than that of the pore-lining chlorite (Fig. 10A, B, D). Studies have shown that in diagenetic systems, the Si, Al^{VI}, and Si/Al contents systematically decrease, and the Sum (VI) and Al^{IV} contents increase with depth or temperature (Jahren, 1991; Zhang et al., 2012). The formation temperature of pore-lining chlorite may be lower than that of pore-filling chlorites, which is in accordance with the fluid inclusion results.

A negative correlation exists between Fe + Al^{VI} and Mg (Fig. 11A) ($R^2 = 0.56$, 0.50), indicating that the octahedron is occupied by Fe, Mg, and Al. The correlation between Fe and Al^{VI} is the strongest ($R^2 = 0.97$, 0.90) among the three ions (Fig. 11B–D), indicating that the substitution of Al by Fe mainly occurred on the octahedron, and chlorite developed in a comparatively Fe-rich environment (Zhou Du et al., 2018).

The existence of iron in clastic sediments is the key to the formation of chlorite in sandstone (Zhu et al., 2017; Worden et al., 2020). Therefore, it is crucial to determine the iron source of chlorite in the study area. VRFs and biotites are abundant in the tight sandstone, with an average content of over 11.5%. Chlorite and VRFs are positively correlated (Fig. 12A). In addition, the BSE observations reveal that the titanium-rich oxides related to volcanic materials are positively correlated with the chlorite (Fig. 13). It is generally believed that titanium originates from volcanic materials or biotites (Bahlis and Ros, 2013). Titanium is a tetravalent ion, which is incompatible with the chlorite lattice structure; therefore, titanium-rich minerals precipitate in the pores surrounding the chlorite cements (Bahlis and Ros, 2013). The results of energy spectrum scanning also show that titanium is positively correlated with the chlorite content (Fig. 12B). In addition, the

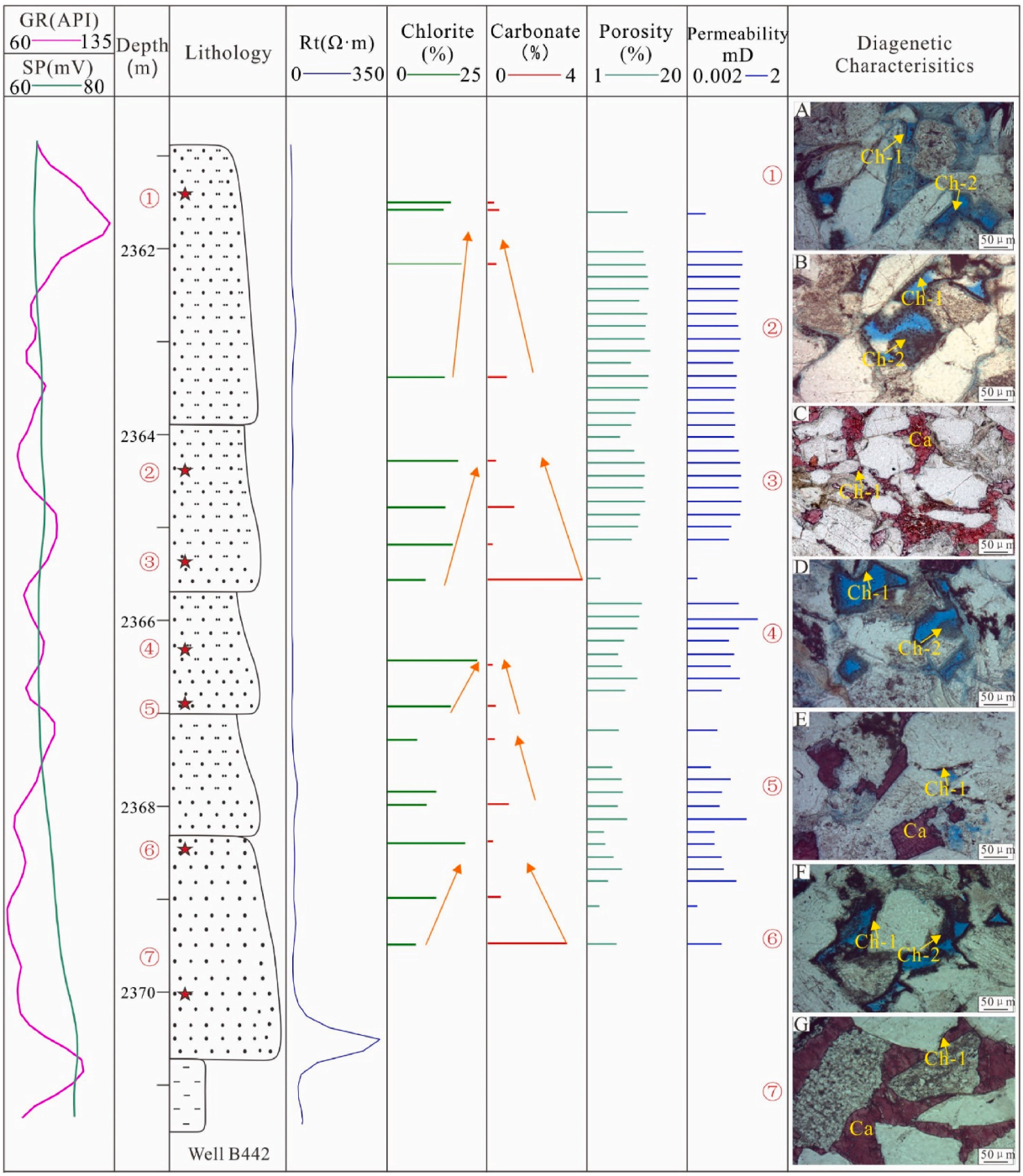

Fig. 6. Distribution characteristics of the chlorite in the reservoir sandstones of the Upper Triassic Yanchang Formation (modified from Xi et al., 2019b); the figure shows the Chang 9 member, and the asterisk in the lithology column indicates the thin section points. (A, B, D, F) Photomicrograph of thin sections showing pore-lining chlorite (Ch-1) and pore-filling chlorite (Ch-2) in the middle to upper part of the fining-upward sandstones. (C, E, G) Photomicrograph of thin sections showing calcite (Ca) with pore-lining chlorite (Ch-1) in the bottom part of the fining-upward sandstones.

observations of the thin sections indicate that chlorite is well developed near the dissolution of VRFs (Fig. 6). These results show that the primary source of main ions for chlorite authigenesis is the alteration of volcanic fragments and biotites.

5.2.1. *Origin of pore-lining chlorite*

The pore-lining chlorite has the same characteristics as the precursor clay rims. The pore-lining chlorite occurs as flaky plates, and the crystal formation is poor. In addition, small and irregularly shaped chlorite is often observed growing under the chlorite flakes, resulting in double layers of the pore-lining chlorite (Fig. 15C). There are two main views on the formation of pore-lining chlorite in sandstone, i.e., the transformation of clay mineral precursors and direct precipitation from pore waters. It is unlikely that the chlorite with poor crystallization formed by direct crystallization from pore waters; thus, the pore-lining chlorite could indicate an origin from precursor clay rims.

The EPMA analysis indicates that the ratio of Al/Fe + Mg + Al of the pore-lining chlorites is 0.39–0.46, with an average of 0.43. In mineralogy, the ratio of Al/Fe + Mg + Al is often used to determine the source of chlorite (Laird, 1988). It is generally believed that chlorite derived

Table 1
Results of the electronic probe microanalysis of chlorite from the tight sandstone reservoir in the Upper Triassic Yanchang Formation.

Well	Depth, m	Member	Type of Chlorite	Results of the Electronic Probe Microanalysis, %										
				Na_2O	MgO	Al_2O_3	SiO_2	K_2O	CaO	TiO_2	FeO	MnO	Cr_2O_3	Total
L28	1703.85	Ch9	Ch-1	0.15	6.27	16.86	19.05	0.12	0.20	0.03	16.19	0.24	0.03	59.12
L28	1703.85	Ch9	Ch-1	0.06	6.15	16.05	19.23	0.08	0.09	0.06	18.90	0.28	0.02	60.92
L28	1703.85	Ch9	Ch-1	0.17	6.84	17.33	20.80	0.08	0.13	0.00	18.36	0.25	0.00	63.96
L28	1703.85	Ch9	Ch-1	0.09	6.40	17.42	19.74	0.09	0.19	0.03	20.34	0.30	0.02	64.59
L28	1703.85	Ch9	Ch-1	0.08	6.51	17.25	22.32	0.19	0.18	0.03	19.32	0.21	0.02	66.10
L28	1671.92	Ch8	Ch-1	0.05	5.55	14.09	17.04	0.01	0.25	0.04	14.94	0.15	0.06	53.17
L28	1703.85	Ch9	Ch-1	0.05	8.10	20.97	25.85	0.25	0.17	0.01	24.20	0.32	0.02	79.93
L28	1703.85	Ch9	Ch-1	0.15	5.81	16.38	19.56	0.10	0.16	0.01	22.48	0.31	0.06	65.01
W64	2202.70	Ch9	Ch-2	0.04	9.40	20.31	25.49	0.01	0.12	0.00	28.94	0.39	0.03	84.73
W64	2202.70	Ch9	Ch-2	0.00	10.93	21.07	27.47	0.02	0.15	0.02	27.79	0.44	0.06	87.94
W64	2202.70	Ch9	Ch-2	0.11	8.31	15.65	20.81	0.05	0.15	0.05	26.60	0.41	0.06	72.20
W64	2202.70	Ch9	Ch-2	0.05	9.51	19.93	24.66	0.02	0.11	0.06	27.74	0.44	0.05	82.57
W64	2202.70	Ch9	Ch-2	0.06	9.43	18.48	24.61	0.03	0.13	0.00	26.59	0.41	0.10	79.85
B442	2350.00	Ch9	Ch-2	0.13	9.86	18.72	25.37	0.05	0.19	0.00	23.34	0.39	0.03	78.08
B442	2350.00	Ch9	Ch-2	0.19	9.59	18.84	24.00	0.05	0.16	0.01	23.55	0.37	0.02	76.77
B442	2350.00	Ch9	Ch-2	0.07	10.09	19.47	25.31	0.03	0.15	0.03	23.57	0.37	0.02	79.11
B442	2350.00	Ch9	Ch-2	0.09	9.23	18.25	23.64	0.07	0.10	0.00	22.05	0.35	0.04	73.82
B442	2350.00	Ch9	Ch-2	0.09	8.30	16.94	22.15	0.04	0.12	0.03	21.09	0.43	0.03	69.21
B442	2350.00	Ch9	Ch-2	0.13	9.96	18.89	24.61	0.03	0.19	0.02	24.59	0.37	0.03	78.84
B442	2350.00	Ch9	Ch-2	0.08	8.45	16.66	21.53	0.01	0.12	0.01	21.00	0.43	0.07	68.35
B442	2350.00	Ch9	Ch-2	0.10	9.83	18.70	24.63	0.05	0.23	0.04	24.06	0.37	0.02	78.02
B442	2350.00	Ch9	Ch-2	0.14	11.05	21.69	27.46	0.05	0.09	0.00	24.77	0.46	0.02	85.72
B442	2350.00	Ch9	Ch-2	0.05	8.46	15.42	21.21	0.12	0.23	0.04	18.44	0.32	0.02	64.31
B442	2350.00	Ch9	Ch-2	0.07	8.64	17.13	22.62	0.02	0.09	0.04	18.18	0.34	0.01	67.15

Table 2
The results of the structural analysis of chlorite from the tight sandstone reservoir in the Upper Triassic Yanchang Formation.

Well	Depth, m	Member	Type of chlorite	Element													
				Na	Mg	Al	Al^{IV}	Al^{VI}	Si	K	Ca	Ti	Fe	Mn	Cr	Fe/Fe + Mg	Al/Fe + Mg + Al
L28	1703.85	Ch9	Ch-1	0.18	2.88	6.08	2.18	3.90	5.82	0.09	0.06	0.01	4.14	0.06	0.01	0.59	0.46
L28	1703.85	Ch9	Ch-1	0.08	2.79	5.73	2.17	3.56	5.83	0.06	0.03	0.01	4.79	0.07	0.00	0.63	0.43
L28	1703.85	Ch9	Ch-1	0.19	2.92	5.81	2.08	3.73	5.92	0.06	0.04	0.00	4.37	0.06	0.00	0.60	0.44
L28	1703.85	Ch9	Ch-1	0.10	2.76	5.89	2.33	3.56	5.67	0.06	0.06	0.01	4.88	0.07	0.00	0.64	0.44
L28	1703.85	Ch9	Ch-1	0.08	2.69	5.60	1.86	3.74	6.14	0.13	0.05	0.01	4.45	0.05	0.00	0.62	0.44
L28	1671.92	Ch8	Ch-1	0.06	2.90	5.78	2.06	3.72	5.94	0.01	0.09	0.01	4.35	0.04	0.02	0.60	0.44
L28	1703.85	Ch9	Ch-1	0.04	2.79	5.68	2.06	3.62	5.94	0.15	0.04	0.00	4.65	0.06	0.00	0.62	0.43
L28	1703.85	Ch9	Ch-1	0.17	2.53	5.61	2.31	3.30	5.69	0.08	0.05	0.00	5.47	0.08	0.01	0.68	0.41
W64	2202.70	Ch9	Ch-2	0.04	3.14	5.33	2.32	3.01	5.68	0.00	0.03	0.00	5.39	0.07	0.01	0.63	0.38
W64	2202.70	Ch9	Ch-2	0.00	3.47	5.25	2.19	3.06	5.81	0.01	0.03	0.00	4.91	0.08	0.01	0.59	0.39
W64	2202.70	Ch9	Ch-2	0.11	3.33	4.93	2.44	2.49	5.56	0.04	0.04	0.01	5.94	0.09	0.01	0.64	0.34
W64	2202.70	Ch9	Ch-2	0.05	3.26	5.36	2.37	2.99	5.63	0.01	0.03	0.01	5.29	0.08	0.01	0.62	0.39
W64	2202.70	Ch9	Ch-2	0.06	3.33	5.13	2.21	2.92	5.79	0.02	0.03	0.00	5.23	0.08	0.02	0.61	0.37
B442	2350.00	Ch9	Ch-2	0.12	3.48	5.20	2.02	3.17	5.98	0.03	0.05	0.00	4.60	0.08	0.01	0.57	0.39
B442	2350.00	Ch9	Ch-2	0.18	3.47	5.35	2.21	3.14	5.79	0.03	0.04	0.00	4.75	0.08	0.00	0.58	0.39
B442	2350.00	Ch9	Ch-2	0.06	3.52	5.33	2.12	3.21	5.88	0.02	0.04	0.01	4.58	0.07	0.00	0.57	0.40
B442	2350.00	Ch9	Ch-2	0.08	3.45	5.36	2.11	3.25	5.89	0.04	0.03	0.00	4.59	0.07	0.01	0.57	0.40
B442	2350.00	Ch9	Ch-2	0.09	3.32	5.32	2.09	3.23	5.91	0.03	0.03	0.01	4.70	0.10	0.01	0.59	0.40
B442	2350.00	Ch9	Ch-2	0.12	3.52	5.24	2.20	3.04	5.80	0.02	0.05	0.00	4.84	0.07	0.01	0.58	0.39
B442	2350.00	Ch9	Ch-2	0.09	3.43	5.31	2.17	3.14	5.83	0.00	0.03	0.00	4.76	0.10	0.01	0.58	0.39
B442	2350.00	Ch9	Ch-2	0.09	3.50	5.23	2.15	3.08	5.85	0.03	0.06	0.01	4.78	0.07	0.00	0.58	0.39
B442	2350.00	Ch9	Ch-2	0.12	3.54	5.45	2.14	3.31	5.86	0.03	0.02	0.00	4.42	0.08	0.00	0.56	0.41
B442	2350.00	Ch9	Ch-2	0.06	3.61	5.17	1.97	3.19	6.03	0.09	0.07	0.01	4.38	0.08	0.01	0.55	0.39
B442	2350.00	Ch9	Ch-2	0.07	3.48	5.42	1.92	3.50	6.08	0.02	0.03	0.01	4.08	0.08	0.00	0.54	0.42

from mafic rocks or their fragments has a lower ratio than that related to mudstone and mud fragments or clay mineral transformation. This result also show that the pore-lining chlorite may have originated from the precursor clay mineral. Moreover, the XRD analysis shows an apparent negative correlation between the content of the I/S mixed layer and the chlorite content (Fig. 14). The correlation coefficients of the Chang 8 and Chang 9 members are 0.7016 and 0.8438, respectively. This negative relationship indicates that the chlorites in the two members likely have the same source. The I/S is an intermediate product of smectite and illite; therefore, it is likely that both the I/S and the chlorite in the sandstone originated from the smectite transformation.

It is believed that volcanic rock fragments in sandstone are easily transformed into smectite (Margarita et al., 2010; Sun et al., 2020). Previous studies have shown that smectite can transform into chlorite in an alkaline environment enriched in iron and magnesium and illite in a potassium-rich environment (Shabani, 2011; Li Y. et al., 2017; Du et al., 2018). The content of potassium feldspar is very low in the tight sandstone, with an average content of 6.6%, and the potassium feldspar is not entirely dissolved. Thus, the transformation from smectite to illite would be difficult. However, the sandstones are rich in mafic fragments, which can provide a large amount of iron and magnesium ions during the burial process, facilitating the transformation of smectite to chlorite. It is also observed that tiny and irregular chlorite formed on the dissolution surface of the fragments (Fig. 15A and B.), which provides direct

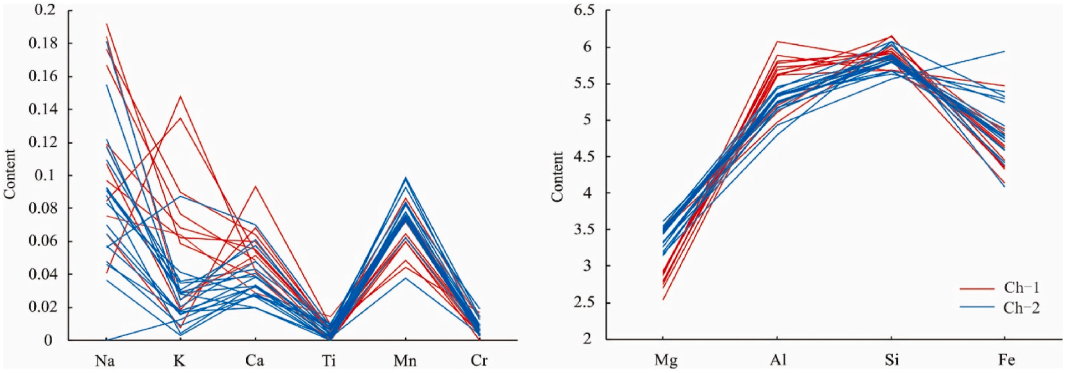

Fig. 7. Elemental geochemistry of the two types of chlorite in the reservoir sandstone of the Upper Triassic Yanchang Formation.

Table 3
Microthermometric data of the fluid inclusions in the upper triassic yanchang sandstone reservoirs.

Well	Depth, m	Th, °C	Number	Diagenetic Mineral
C107	2312.5	86.2–96.4/91.6	3	Ca–I
C107	2309.15	81.8–96.7/89.2	2	Ca–I
Y465	2377.3	97.6–111.4/106.9	3	Ca-II
L28	1698.73	90.1–100.9/93.8	3	Qo-I
L28	1706.4	98.3–103.9/101.1	2	Qo-I
Y465	2381.65	97.2–108/102.6	2	Qo-I
C107	2309.15	89.3–95.1/92.2	2	Qo-I
L28	1706.4	119.2–122.2/120.8	3	Qo-II

"86.2–96.4/91.6" = minimum-maximum/average values of the homogenization temperature of the aqueous inclusions; Th= Homogenization temperature (Th). Ca–I = calcite cements without chlorite; Ca-II = calcite cements with chlorite coatings; Qo-I = quartz overgrowths; Qo-II = authigenic quartz grains.

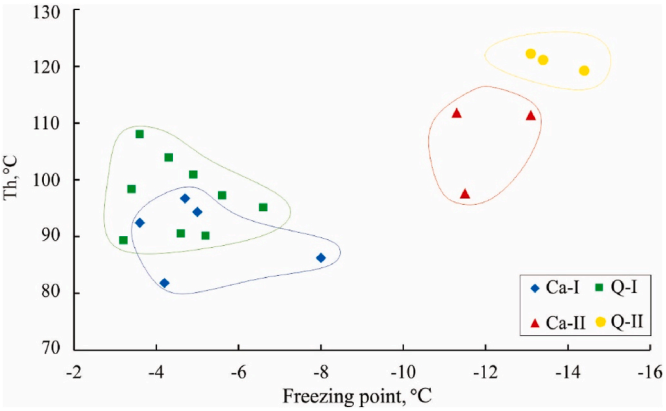

Fig. 8. Homogenization temperature (Th) of the fluid inclusions in the diagenetic minerals in the reservoir sandstone of the Upper Triassic Yanchang Formation.

evidence for the transformation reaction. The quantitative statistics of the EPMA data show that the concentrations of Mg and Si increase with increasing Al content in the pore-lining chlorite, whereas the correlations between the concentrations of Fe and Al, as well as K, are weaker or the points in the plot are scattered (Fig. 17). These results indicate that during the crystallization of early chlorite, Mg and Si were incorporated into the pore-lining chlorite cement together with Al, but Fe, K, and Al ions were not incorporated. The chemical formula of smectite is $(Al_2\text{-}xMgx)_2[Si_4O_{10}]$ $(OH)_2$. nH_2O, indicating that smectite does not contain Fe or K. In other words, most of the Al, Mg, and Si sources in the pore-lining chlorite were present, but Fe and K sources were not. These results support our assumption that the pore-lining chlorite originated

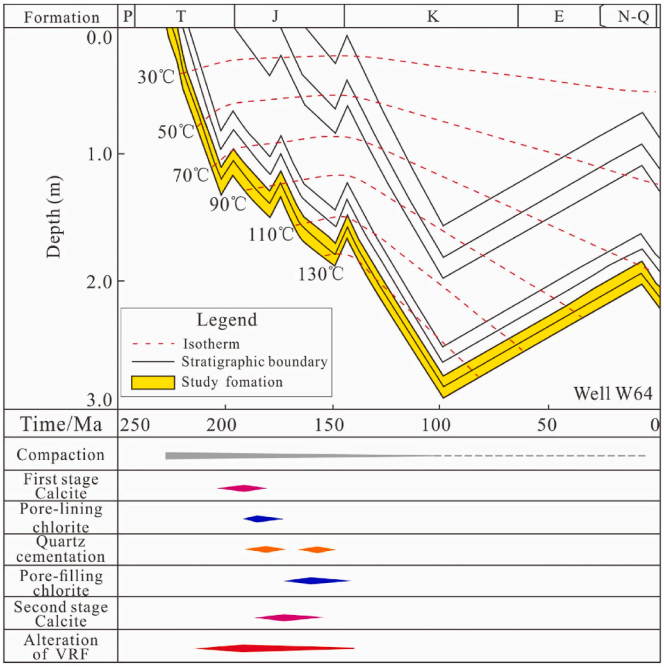

Fig. 9. Burial, thermal, and diagenetic histories of the tight sandstone reservoirs in the Upper Triassic Yanchang Formation (modified from Li et al. (2012)).

from the transformation of smectite.

However, the pore-lining chlorite does not occur as honeycomb-shaped crystalline aggregates which demonstrate that smectite transformation occurred (Hillier et al., 1996). It is likely that the smectite was completely transformed, which is supported by the fact that no mixed-layer chlorite/smectite was detected in the XRD analysis. Moreover, some researchers found honeycomb chlorite in the Yanchang Formation (Zhou et al., 2017), proving the source of precursor clay transformation. The changes in the properties of the pore-lining chlorite at different sites resulted from growth by geometric selection (Billault et al., 2003). In other words, the pore-lining chlorite was the result of a single crystallization stage that was controlled by geometric selection. In the crystallization stage, space competition occurred between chlorite crystals. The crystal orientation was conducive to growth. Therefore, only the chlorite whose growth direction was perpendicular to the growth surface could continue to grow, explaining why the chlorite is often vertically distributed on the mineral surface.

In summary, the pore-lining chlorite was derived from the precursor clay mineral (smectite) formed by volcanic fragments. The provenance of the study area is rich in volcanic debris, which was transported to the

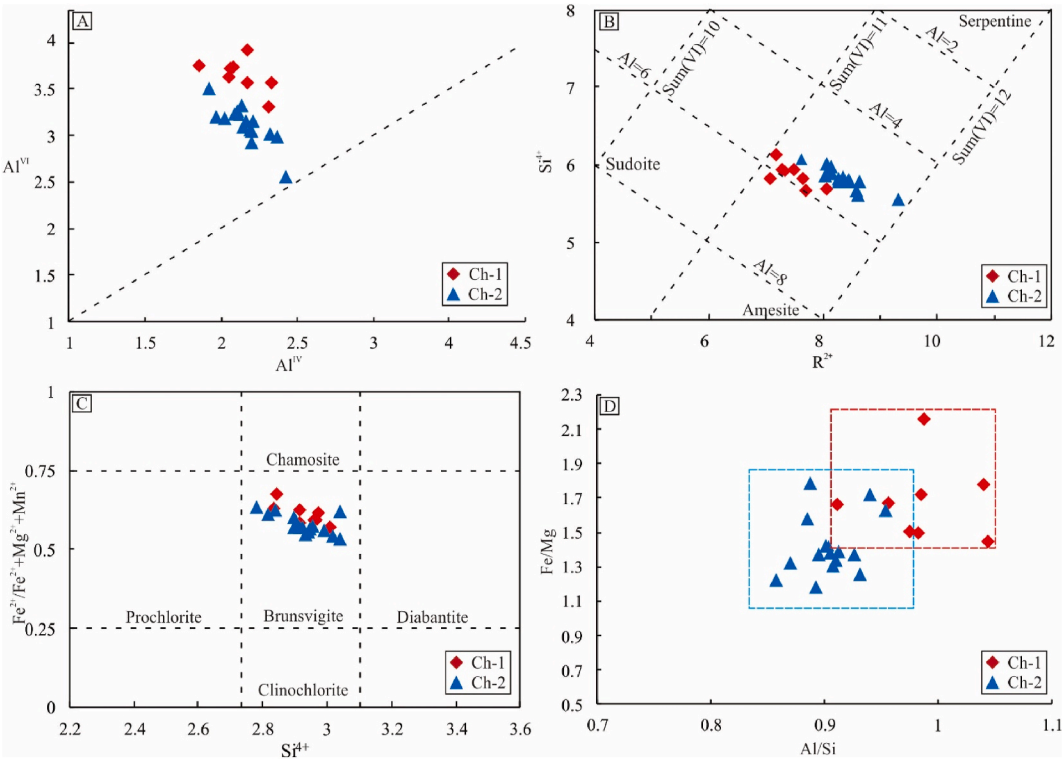

Fig. 10. Element characteristics of chlorite in the tight sandstone reservoirs of the Upper Triassic Yanchang Formation. (A) Correlation of main cations of chlorite. (B) The formula of chlorite according to the model system (Wiewiora and Weiss, 1990). (C) Chlorite classification system of Foster (1962), showing the type of chlorites. (D) Correlation between the ratio of Fe/Mg and Al/Si.

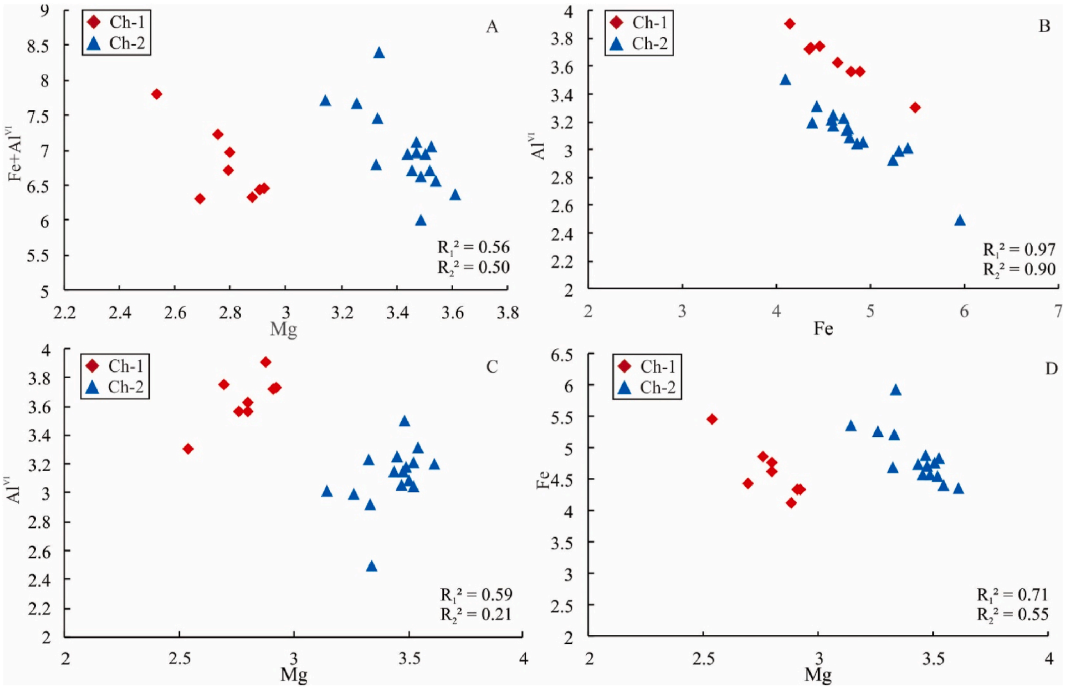

Fig. 11. Relationship between the primary cations of chlorites in the tight sandstone reservoirs of the Upper Triassic Yanchang Formation. (A) Correlation between the Fe + Al^{VI} and Mg, indicating that the octahedron is occupied by Fe, Mg, and Al; (B–D) Correlation between the Al^{VI}, Fe, and Mg.

study area by the rivers (Huang et al., 2004; Luo et al., 2008; Ding et al., 2013). In the early burial period, the volcanic materials were unstable and were easily transformed into smectite. As the burial depth increased, the precursor clay became unstable, and iron and magnesium ions were provided by the dissolution of VRF to enable the transformation to chlorite.

5.2.2. *Origin of pore-filling chlorite*

The pore-filling chlorite occurs as euhedral pseudo-hexagonal crystals, with a thickness of more than 8 μm. The crystal form and size are

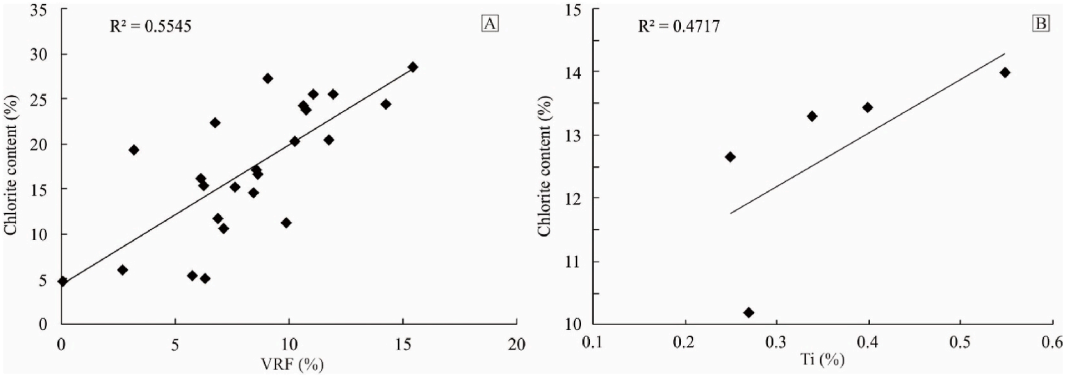

Fig. 12. Correlation of the chlorite content with the (A) volcanic rock fragment content and (B) titanium content.

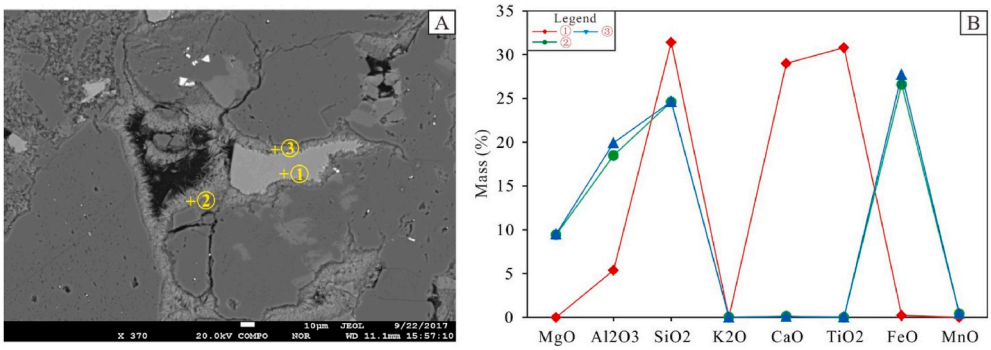

Fig. 13. Results of the in situ microprobe analysis of the pore-lining chlorite and titanium-rich oxides. (A) Backscattered electron image showing the analysis locations of the W64 sample (2202.7 m). (B) The ion concentrations at the locations in the backscattered electron image shown in (A).

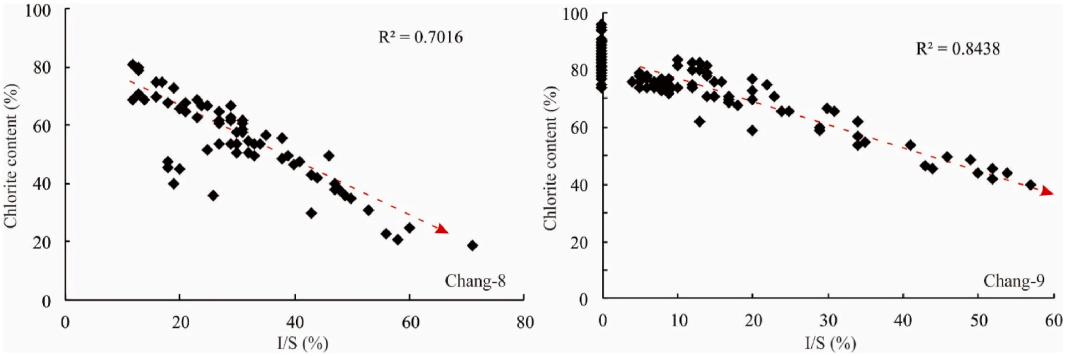

Fig. 14. Correlation between the chlorite content and the illite/smectite (I/S) content.

different from those of the pore-lining chlorite, indicating that the pore-filling chlorite had sufficient time and space to crystallize. The EPMA data indicates that the Al/Fe + Mg + Al ratio of the late chlorite is 0.34–0.42, with an average of 0.39. This ratio is significantly lower than that of the pore-lining chlorite. Although the ratio is higher than 0.35, the chlorite did not originate from clay because the distribution and morphology are distinct. Studies have shown that the development of chlorite is a process of continuous rebalancing with the environment (Grigsby, 2001), indicating that the composition of the chlorite largely depended on the properties of the paleo-fluids in the sandstone reservoirs. Generally, chlorite formed by the transformation of clay mineral precursors has inherited characteristics, and the crystal formation tends to be poor. Therefore, it is assumed that the pore-filling chlorite was precipitated directly in pore spaces from pore water with high concentrations of Mg^{2+} and Fe^{2+}. Haile et al. (2015) used clean feldspar, quartz particles, and artificial formation water as raw materials to simulate the growth of chlorite in experiments. At about 100 °C, chlorite was successfully formed, which confirmed that chlorite could be precipitated from pore waters under appropriate conditions. The precipitation temperature of pore-filling chlorite in the study area is about 110 °C (Fig. 9), satisfying the temperature conditions for chlorite formation. At the microscopic level, it is found that chlorite developed by the dissolution of volcanic rock debris and mica (Fig. 15D–F), supporting that the origin may be related to the fragments or micas.

The quantitative statistics of the EPMA data show a positive correlation between Mg and Fe (R^2 = 0.57) in the pore-filling chlorite (Fig. 16). However, the correlations between the concentration of Mg and Al (R^2 = 0.14) and between Fe and Al (R^2 = 0.37) are weak, and the points in the plot are scattered (Fig. 16). Moreover, the trace ions, such as K and Ca with Mg, are positively correlated (Fig. 16). These results indicate that during the crystallization of pore-filling chlorite, K and Ca in the pore waters were incorporated into the pore-lining chlorite

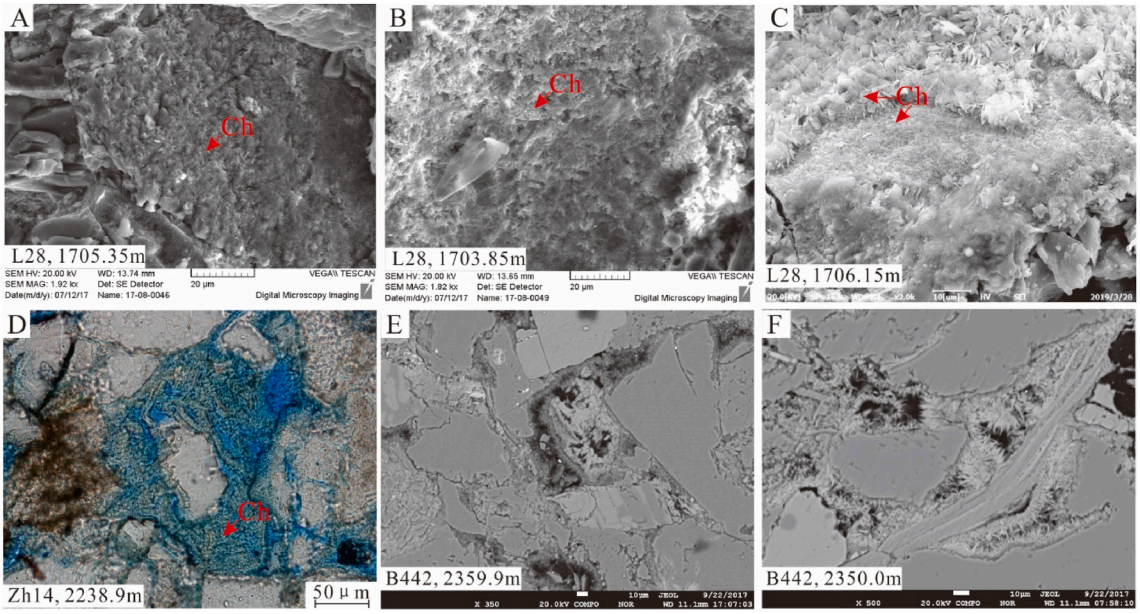

Fig. 15. Characteristics of the chlorite in the Upper Triassic Yanchang Formation. (A–B) Scanning electron microscope images showing the tiny irregular chlorite particles that formed on the dissolution surface of the debris in the L28 sample (1705.3 m, 1703.85 m). (C) Scanning electron microscope image showing double layers of pore-lining chlorite in the L28 sample (1706.15 m). (D) Photomicrographs of thin sections under plane-polarized light showing that the fragments were transformed into chlorite in the Zh14 sample (2238.9 m). (E–F) Backscattered electron (BSE) images showing that the VRF and mica were transformed into chlorite in the B442 sample (2359.9 m, 2350.0 m).

together with Mg. This response may be related to the difference in the ions released by VRF alteration. At low temperatures (about 100 °C), Fe, Mg, K, and Ca were easily released into the pore waters through the dissolution of fragments, whereas Al and Si were relatively difficult to remove (Zhang et al., 2017). This may lead to the enrichment of Fe, Mg, K, and Ca in the pore fluids. Moreover, Mg and Fe are easily transferable ions, whereas Si and Al are not. Nevertheless, the correlation between Mg and Si is strong. There is a weak correlation between Al, Fe, and Mg. This indicates that the ions did not originate from outside sources but from internal sources, i.e., the initial sandstone. The result indicates that the pore-filling chlorite was precipitated directly from pore water with high concentrations of Mg^{2+} and Fe^{2+}.

Unlike the pore-lining chlorite, the pore-filling chlorite does not develop at the bottom of the fining-upward sandstones, where later-stage calcite (Ca-II) cements are abundant. The chlorite is also found in the residual pores where calcite is partially cemented (Fig. 3C). All these results indicate that Ca-II inhibited the growth of pore-filling chlorite. In addition, this result is supported by the significant inverse correlation between the calcite cement and chlorite contents (Fig. 6).

Moreover, the EPMA analysis shows that the calcites are rich in iron and magnesium ions (mainly iron ions) (Fig. 17), whereas the pore-filling chlorite has a low Fe content and a high Mg content (Fig. 7). This result indicates that the Ca-II not only occupied the space where the chlorite was formed but also likely "absorbed" part of the ions preferentially, like magnesium ions. Particle size is a crucial parameter that affects the stress sensitivity of a reservoir (Liu et al., 2020). In comparison, the lower portion of the fining-upward sandstones contains numerous rigid and coarser detrital quartz particles; therefore, the bottom had stronger resistance to compaction than the middle and upper parts. In other words, a "high-porosity and high-permeability zone" was formed at the bottom of the unit due to its stronger resistance to compaction (Xi et al., 2019b). Therefore, the pore water was more active at the bottom of the sand unit, and the volcanic material alteration occurred relatively quickly. In addition, the carbon dioxide created by the decarboxylation of organic matter also preferentially entered the zone, causing extensive Ca-II precipitation at the bottom of the sand unit (Xi et al., 2019b). Moreover, part of the Fe^{2+} and Mg^{2+} in the pore water was removed by the early Ca-II, which resulted in insufficient sources for the growth of the pore-filling chlorite. It was not until the precipitation of calcite was complete that chlorite began to slowly precipitate out of the pore water rich in iron and magnesium. However, the early Ca-II occupied the growth space of the chlorite, and the pore-filling chlorite could only grow in the residual pores after calcite cementation (Fig. 3C).

In the middle and upper part of the fining-upward sandstones, less pore water activity occurred due to lower porosity and permeability, which slowed the alteration rate of the VRFs. However, due to the alteration, the contents of Fe, Mg, Al, and Si gradually increased in the pore water, but calcite could not form due to a lack of carbon source. When suitable conditions occurred, pore-filling chlorite began to precipitate from the pore waters. Unlike the pore-lining chlorite, the pore-filling chlorite did not have precursor clay, and the fragments were dissolved while supplying the source; thus, the pore-filling chlorite crystallized slowly. The temperature of this process was high, and the resulting crystals were large and had good crystal morphology. This process resulted in the inhomogeneous distribution of pore-filling chlorite, which only occurred in the middle to upper part of the fining-upward sandstones. Because of the different migration properties of the ions, the pore-filling chlorite was commonly concentrated near the Fe, Si, and Al sources.

5.3. Implications for reservoir quality

There is no doubt that the effect of pore-filling chlorite on reservoirs is negative because it can plug pores and pore throats (Fig. 2B). However, there is debate regarding the implications of pore-lining chlorite for reservoir quality. Although some researchers have raised that pore-lining chlorite also has negative implications for reservoir quality (Yao et al., 2011; Xiang et al., 2016; Ma et al., 2017a; Zhou et al., 2017), it is generally agreed that pore-lining chlorite can preserve reservoirs by restricting the growth of quartz cement (Ehrenberg, 1993; Hillier et al., 1996; Billault et al., 2003; Huggett et al., 2015; Cao et al., 2017; Zhu et al., 2017). Pore-lining chlorite can restrict the growth of quartz cement, especially quartz overgrowth, by retarding quartz nucleation

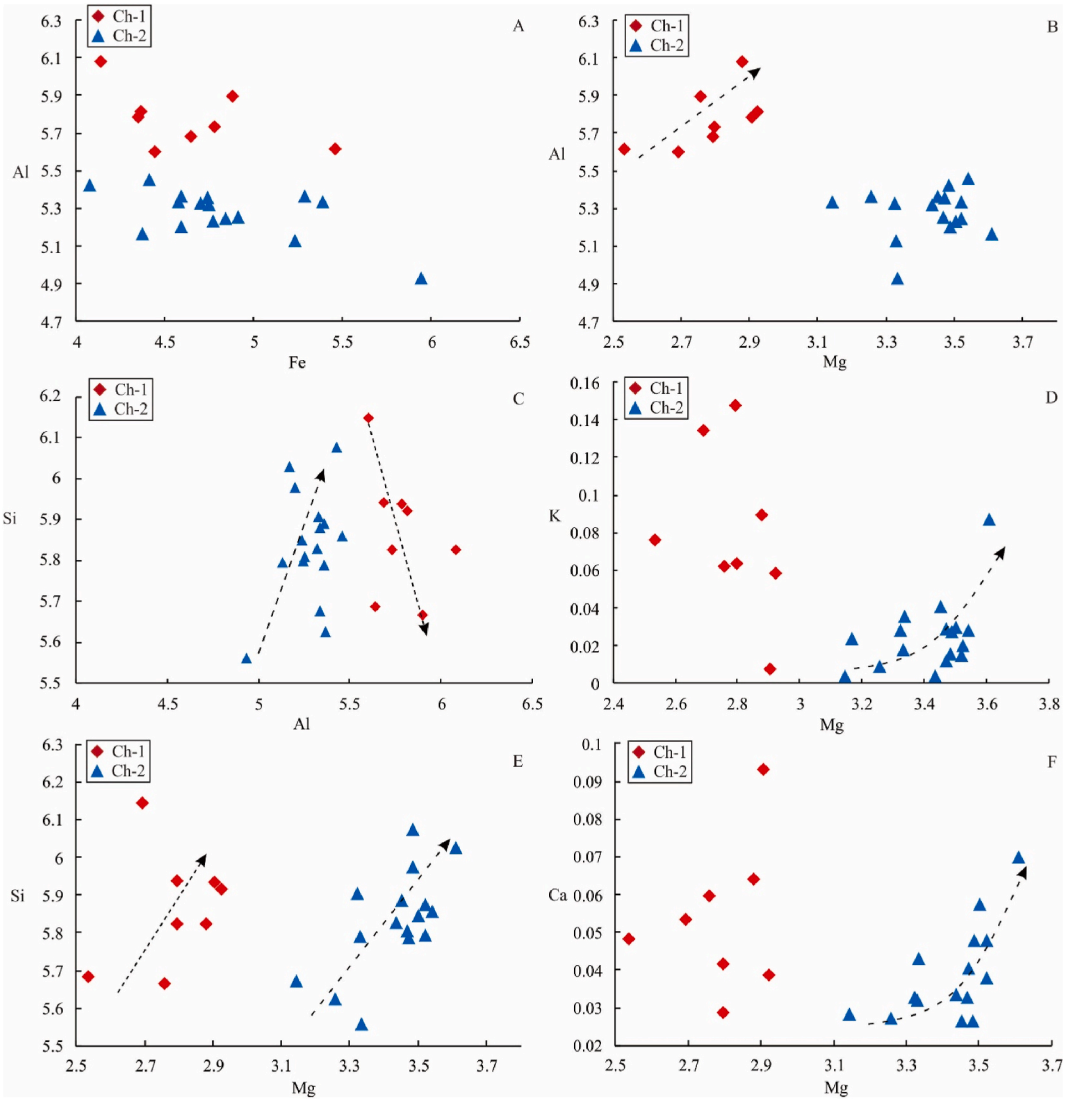

Fig. 16. Correlation between the main cations in the chlorite tight sandstone reservoirs of the Upper Triassic Yanchang Formation.

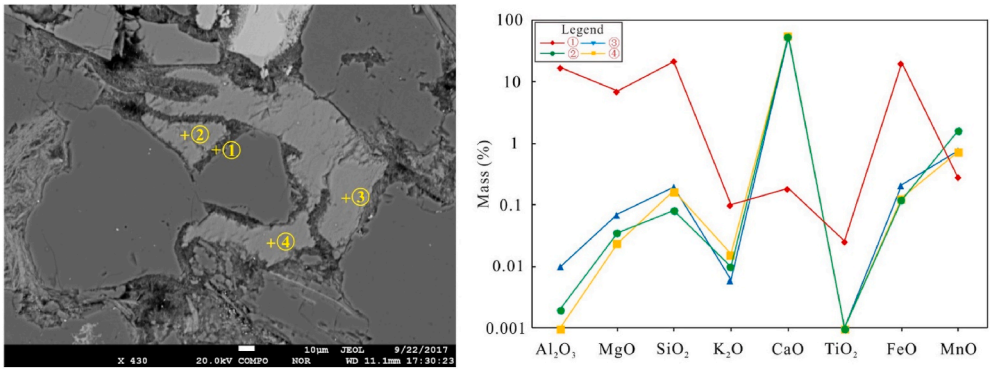

Fig. 17. Results of the in situ microprobe analysis of the pore-lining chlorite and calcite. (A) Backscattered electron image showing the analysis locations of the W64 sample (2202.7 m). (B) The ion concentrations at the locations in the backscattered electron image.

(Ehrenberg, 1993; Grigsby, 2001; Ajdukiewicz and Richard, 2012) or occupying the growth space of authigenic quartz (Billault et al., 2003).

In the Chang 8 and Chang 9 sandstones, the quartz overgrowth is rarely observed in locations of pore-lining chlorite development (Fig. 18A). The SEM observations also shows that quartz overgrowth only developed in locations where the pore-lining chlorite was discontinuous or the chlorite was very thin (Fig. 18B). In addition, there is an inverse correlation between the chlorite content and the quartz cement content (Fig. 18C). Therefore, it appears that the pore-lining chlorite inhibited quartz cementation.

Pore-lining chlorite is common in the Chang 8 and Chang 9 sandstones, but has different thicknesses. The thickness of the chlorite may

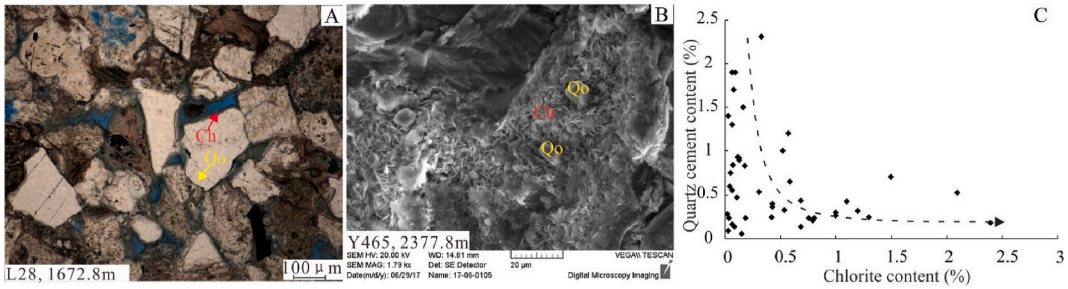

Fig. 18. Correlation between chlorite and quartz. (A) Photomicrographs of thin sections under plane-polarized light showing pore-lining chlorite with quartz overgrowth for the L28 sample (1672.8 m). (B) Scanning electron microscope image showing the relationship between chlorite and quartz overgrowth in the Y465 sample (2377.8 m). (C) Correlation between chlorite and quartz cement.

be a suitable parameter for evaluating its impact on reservoir quality. The statistical results show that the porosity increases first and then decreases as the thickness increases (Fig. 19A), and the permeability is generally lower when the thickness is below 4.5 μm or higher than 6.7 μm (Fig. 19B). This result demonstrates that an appropriate thickness of the pore-lining chlorite can preserve the reservoir quality; however, if the pore-lining chlorite is too thick, it occupies too much pore space and throats (Fig. 4A), thereby reducing sandstone porosity and permeability. If the pore-lining chlorite is too thin, it cannot effectively inhibit the growth of quartz cement (Fig. 18), which is not enough to protect reservoirs quality.

Moreover, a correlation exists between the total content of authigenic chlorite and the porosity and permeability. The porosity increases first and then decreases as the chlorite content increases (Fig. 20A), and the permeability is generally lower when the chlorite content is below 16% or above 25% (Fig. 20B). This relationship indicates that when the content of authigenic chlorite is low, it may occur primarily as pore-lining chlorite. The chlorite content increases as the thickness of the pore-lining chlorite increases, and an appropriate thickness is conducive to good reservoir quality (Fig. 19). However, a high chlorite content results in low porosity and permeability, regardless of the chlorite type. As the content increases, the pore-filling chlorite and pore-lining chlorite fills the pores, destroying reservoir quality. The reservoir has the best properties when the total chlorite content is between 16% and 20%.

6. Conclusions

More attention should be paid to the heterogeneity of rock composition and diagenesis under a sandstone sequence, in order to better predict the reservoir qualities of tight sandstones. As a common clay mineral in tight sandstone reservoirs, authigenic chlorite has an indication of reservoir quality. An in-depth study of authigenic chlorite, including the types and the genesis, can better understand the reservoir heterogeneity and provide some guidance for tight oil development.

Two types of authigenic chlorite, occurring as pore-lining and pore-filling chlorite, were observed in the tight sandstones of the Upper Triassic Yanchang Formation. Pore-lining chlorite was the primary authigenic chlorite, occurring as clay coatings on the framework grains, which grew perpendicular to the particle surface, with a thickness of about 3–10 μm. Pore-filling chlorite occurred as discrete flaky plates or rosette-shaped crystalline aggregates, with a thickness of more than 8 μm.

The pore-lining chlorite originated from smectite precursors that were derived from the alteration of volcanic materials in the early stage of diagenesis, with temperatures below 90 °C. The pore-filling chlorite, in contrast, was precipitated in pore spaces, with higher concentrations of Mg^{2+} and Fe^{2+}, which were released from VRF and mica debris dissolution occurring at temperatures of about 110 °C.

The pore-lining chlorite generally occurred in the fining-upward sandstones, whereas the pore-filling chlorite only formed in the middle to top parts of the fining-upward sandstones. The bottom of the fining-upward sandstones contained numerous rigid and coarse detrital quartz particles, resulting in strong resistance to compaction. The development of the second-stage calcite cements influenced the distribution of the pore-filling chlorite.

Thin and continuous pore-lining chlorite inhibited quartz cementation, preserving the porosity and permeability. However, a large thickness of the pore-lining chlorites (>6.7 μm) or pore-filling chlorite significantly reduced porosity and permeability.

Author contribution

Ke Li: Data curation, Writing – original draft. Kelai Xi: Conceptualization, Methodology, Supervision. Yingchang Cao: Review & Editing, Supervision. Xiaobin Niu: Resources. Songtao Wu: Review & Editing. Shengbin Feng: Resources. Yuan You: Resources.

Declaration of competing interest

The authors declare that they have no known competing financial interests or personal relationships that could have appeared to influence the work reported in this paper.

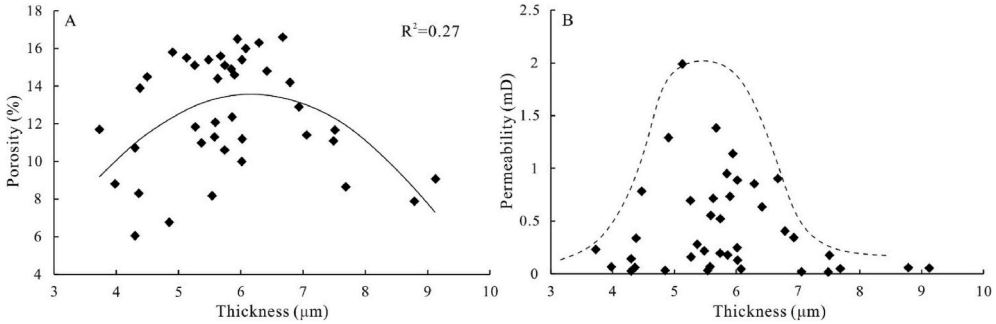

Fig. 19. Correlation between the thickness of the pore-lining chlorite and the (A) porosity and (B) permeability.

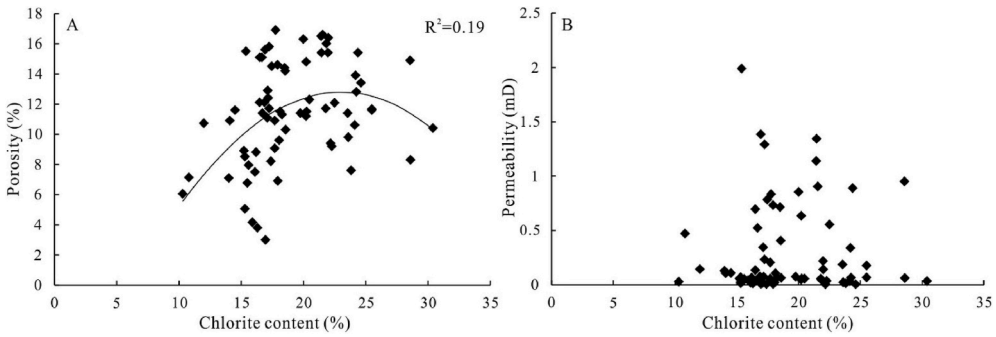

Fig. 20. Correlation between the chlorite content and the (A) porosity and (B) permeability.

Acknowledgments

This study was funded by the National Natural Science Foundation of China (Grants No. U1762217, 42072161), the Innovation Research Group of the Natural Fund Committee (Grant No. 41821002), the Fundamental Research Funds for the Central Universities (Grant No. 19 C × 02009 A), and the Opening Foundation of the State Key Laboratory of Continental Dynamics (16LCD04). We are also thankful to the Changqing Oilfield Company, PetroChina, for providing their in-house database and permission to publish.

Appendix A. Supplementary data

Supplementary data to this article can be found online at https://doi.org/10.1016/j.petrol.2021.108843.

References

Ajdukiewicz, J.M., Larese, R.E., 2012. How clay grain coats inhibit quartz cement and preserve porosity in deeply buried sandstones: observations and experiments. AAPG (Am. Assoc. Pet. Geol.) Bull. 96, 2091–2119.
Anjos, S.M.S., De Ros, L.F., Silva, C.M.A., 2003. Chlorite authigenesis and porosity preservation in the upper cretaceous marine sandstones of the santos basin, offshore eastern Brazil. Special Publ. Int. Assoc. Sedimentol. 34, 291–316.
Bahlis, A.B., De Ros, Luiz, F., 2013. Origin and impact of authigenic chlorite in the Upper Cretaceous sandstone reservoirs of the Santos Basin, eastern Brazil. Petrol. Geosci. 19, 185–199.
Berger, A., Gier, S., Krois, P., 2009. Porosity-preserving chlorite cements in shallow-marine volcaniclastic sandstones: evidence from Cretaceous sandstones of the Sawan gas field, Pakistan. AAPG (Am. Assoc. Pet. Geol.) Bull. 93, 595–615.
Billault, V., Beaufort, D., Baronnet, A., Lacharpagne, J.C., 2003. A nanopetrographic and textural study of grain-coating chlorites in sandstone reservoirs. Clay Miner. 38, 315–328.
Cao, Z., Liu, G., Meng, W., Wang, P., Yang, C., 2018. Origin of different chlorite occurrences and their effects on tight clastic reservoir porosity. J. Petrol. Sci. Eng. 160, 384–392.
Ding, X., Han, M., Liu, Y., Wan, Y., 2013. Coupling relation between provenance and diagenesis of siliciclastic reservoirs in the Yanchang formation, Ordos basin. Geology and Exploration 49, 384–392 (in Chinese with English abstract).
Du, J.Z., Cai, J.G., Xie, Z.H., Wang, X., 2018. Chloritization sequences in mudstone during diagenesis and its geological significance. Geol. J. China Univ. 24, 371–379.
Dutton, P.S., Loucks, G.R., 2010. Diagenetic controls on the evolution of porosity and permeability in lower Tertiary Wilcox sandstones from shallow to ultradeep (200-6700 m) burial, Gulf of Mexico Basin. U.S.A. Mar. Petrol. Geol. 27, 69–81.
Ehrenberg, S.N., 1993. Preservation of anomalously high porosity in deeply buried sandstones by grain coating chlorite examples from the Norwegian continental shelf. AAPG (Am. Assoc. Pet. Geol.) Bull. 77, 1260–1286.
Fan, A., Yang, R., Li, J., Zhao, Z., Van Loon, A.J., 2017. Siliceous cementation of chlorite-coated grains in the permian sandstone gas reservoirs, ordos basin. Acta Geol. Sin. 91, 1147–1148.
Fitch, P.J.R., Lovell, M.A., Davies, S.J., Pritchard, T., Harvey, P.K., 2015. An integrated and quantitative approach to petrophysical heterogeneity. Mar. Petrol. Geol. 63, 82–96.
Folk, R.L., 1974. Petrology of Sedimentary Rocks. Hemphill Publishing Company, Austin, p. 182.
Foster, M.D., 1962. Interpretation of the composition and classification of the chlorites. US Geology Survey Prof 414A, 1–33.
Grigsby, J.D., 2001. Origin and growth mechanism of authigenic chlorite in sandstones of the lower Vicksburg Formation, South Texas. J. Sediment. Res. 71, 27–36.
Gould, K., Pe-piper, G., Piper, D.J.W., 2010. Relationship of diagenetic chlorite rims to depositional facies in Lower Cretaceous reservoir sandstones of the Scotian Basin. Sedimentology 57, 587–610.
Guo, Y., Hui, L., Zhang, X., Wei, Q., Li, W., Li, B., 2018. Sedimentary system characteristics and lake basin evolution of triassic Yanchang formation in Ordos basin. J. NW Univ. 48, 593–602 (in Chinese with English abstract).
Haile, B.G., Hellevang, H., Aagaard, P., Jahren, J., 2015. Experimental nucleation and growth of smectite and chlorite coatings on clean feldspar and quartz grain surfaces. Mar. Petrol. Geol. 68, 664–674.
Hillier, S., 1994. Pore-lining chlorites in siliciclastic reservoir sandstones electron microprobe, SEM and XRD date, and implications for their origin. Clay Miner. 29, 665–679.
Hillier, S., Fallick, A.E., Matter, A., 1996. Origin of pore-lining chlorite in the Aeolian rotliegend of northern Germany. Clay Miner. 31, 153–171.
Hillier, S., 2003. Quantitative analysis of clay and other minerals in sandstones by X-ray powder diffraction (XRPD). Special Publ. Int. Assoc. Sedimentol. 34, 213–251.
Huang, S., Xie, L., Zhang, M., Wu, W., Shen, L., Liu, J., 2004. Formation mechanism of authigenic chlorite and relation to preservation of porosity in nonmarine Triassic reservoir sandstones, Ordos Basin and Sichuan Basin, China. J. Chengdu Univ. Technol. (Sci. Technol. Ed.) 31, 273–281 (in Chinese with English abstract).
Huggett, J.M., Burley, S.D., Longstaffe, F.J., Saha, S., Oates, M.J., 2015. The nature and origin of authigenic chlorite and related cements in oligo-miocene reservoir sandstones, tapti gas fields, surat depression, offshore western India. J. Petrol. Geol. 38, 383–409.
Hu, R., Cao, Y., Xi, K., Mao, Z., Wu, S., Ma, Z., 2018. Sedimentary characteristics of Chang 10-chang 9 oil group in the southern margin of Ordos basin. Pet. Geol. Oilfield Dev. Daqing 37, 31–39 (in Chinese with English abstract).
Jafari, J., Mahboubi, A., Moussavi-Harami, R., Al-Aasm, I.S., 2020. The effects of diagenesis on the petrophysical and geochemical attributes of the Asmari Formation, Marun oil field, southwest Iran. Petrol. Sci. 17, 292–316.
Jahren, J.S., 1991. Evidence of ostwald ripening related recrystallization of diagenetic chlorites from reservoir rocks offshore Norway. Clay Miner. 26, 169–178.
Ju, W., Niu, X., Feng, S., You, Y., Xu, H., 2020. Predicting the present-day in situ stress distribution within the Yanchang Formation Chang 7 shale oil reservoir of Ordos Basin, central China. Petrol. Sci. 17, 912–924.
Karim, A., Piper, P.G., Piper, J.M.D., 2010. Controls on diagenesis of lower cretaceous reservoir sandstones in the western sable subbasin, offshore nova scotia. Sediment. Geol. 224, 65–83.
Lai, J., Wang, G., Ran, Y., Zhang, X., 2015. Depositional and diagenetic controls on pore structure of tight gas sandstone reservoirs: evidence from lower cretaceous bashijiqike formation in kelasu thrust belts, kuqa depression in tarim basin of west China. Resour. Geol. 65, 55–75.
Lai, J., Wang, G., Ran, Y., Zhou, Z., Cui, Y., 2016. Impact of diagenesis on the reservoir quality of tight oil sandstones: the case of Upper Triassic Yanchang Formation Chang 7 oil layers in Ordos Basin, China. J. Petrol. Sci. Eng. 145, 54–65.
Laird, J., 1988. Chlorites: metamorphic petrology. Rev. Mineral. Geochem. 19, 405–453.
Li, M., Guo, Y., Li, Z., Wang, H., 2020. The diagenetic controls of the reservoir heterogeneity in the tight sand gas reservoirs of the Zizhou Area in China's east Ordos Basin: implications for reservoir quality predictions. Mar. Petrol. Geol. 112, 104088.
Li, Y., Cai, J., Wang, X., Hao, Y., Liu, Q., 2017a. Smectite-illitization difference of source rocks developed in saline and fresh water environments and its influence on hydrocarbon generation: a study from the Shahejie Formation, Dongying Depression, China. Mar. Petrol. Geol. 80, 349–357.
Li, Z., Wu, S., Xia, D., Zhang, X., Huang, M., 2017b. Diagenetic alterations and reservoir heterogeneity within the depositional facies: a case study from distributary-channel belt sandstone of Upper Triassic Yanchang Formation reservoirs (Ordos Basin, China). Mar. Petrol. Geol. 86, 950–971.
Liu, B., Yang, Y., Li, J., Chi, Y., Fu, X., 2020. Stress sensitivity of tight reservoirs and its effect on oil saturation: a case study of Lower Cretaceous tight clastic reservoirs in the Hailar Basin, Northeast China. J. Petrol. Sci. Eng. 184, 106484.
Luo, J., Li, Z., Shi, C., Li, J., Han, Y., Wang, H., Li, J., Wang, C., 2008. Depositional systems and provenance dir ectionsfor the Chang 6 and Chang 8 reservoir groups of the Upper Triassic Yanchang Formation in the southwestern Ordos basin, China. Geol. Bull. China 27, 101–111 (in Chinese with English abstract).
Luo, J., Liu, X., Fu, X., Li, M., Kang, R., Jia, K., 2014. Impact of petrologic components and their diagenetic evolution on tight sandstone reservoir quality and gas yield: a

case study from He8 gas-bearing reservoir of upper paleozoic in northern Ordos basin. Earth Sci. J. China Univ. Geosci. 39, 537–544 (in Chinese with English abstract).
Ma, P., Lin, C., Zhang, S., Dong, C., Wei, M., 2017a. An overview on study of chlorite films in clastic reservoirs. J. Palaeogeogr. 19, 147–159 (in Chinese with English abstract).
Ma, P., Lin, C., Zhang, S., Dong, C., Xu, Y., 2017b. Formation of chlorite rims and the impact of pore-lining chlorite on reservoir quality: a case study from Shiqianfeng sandstones in upper Permian of Dongpu Depression, Bohai Bay Basin, eastern China. Aust. J. Earth Sci. 64, 825–839.
Mao, S., Bao, Z., Wang, X., Gao, Y., Song, J., Wang, Z., Liu, W., Zhang, L., Wei, M., Bao, Y., 2019. Origin of carbonate cements and reservoir evolution of tight sandstone in the upper triassic Yanchang formation, Ordos basin, China. Aust. J. Earth Sci. 66, 1–20.
Moore, D.M., Reynolds Jr., R.C., 1999. X-ray diffraction and the identification and analysis of clay minerals. Clay Miner. 34 (1), 210–211.
Murray, H.H., 2006. Applied Clay Mineralogy: Occurrences, Processing and Application of Kaolins, Bentonites, Palygorskite-Sepiolite, and Common Clays. American Cancer Society, p. 180.
Shabani, A.A.T., 2011. Mineral chemistry of chlorite replacing biotite from granitic rocks of the Canadian Appalachians. J. Sci. Islam. Repub. Iran 20, 265–275.
Sun, N., Zhong, J., Hao, B., Ge, Y., Swennen, R., 2020. Sedimentological and diagenetic control on the reservoir quality of deep-lacustrine sedimentary gravity flow sand reservoirs of the Upper Triassic Yanchang Formation in Southern Ordos Basin, China. Mar. Petrol. Geol. 112, 104050.
Wang, G., Chang, X., Yin, W., Li, Y., Song, T., 2017a. Impact of diagenesis on reservoir quality and heterogeneity of the Upper Triassic Chang 8 tight oil sandstones in the Zhenjing area, Ordos Basin, China. Mar. Petrol. Geol. 83, 84–96.
Wang, M., Tang, H., Zhao, F., Liu, S., Lu, H., 2017b. Controlling factor analysis and prediction of the quality of tight sandstone reservoirs: a case study of the He8 Member in the eastern Sulige Gas Field, Ordos Basin, China. J. Nat. Gas Sci. Eng. 46, 680–698.
Wiewióra, A., Weiss, Z., 1990. Crystallochemical classifications of phyllosilicates based on the unified system of projection of chemical composition: II. The chlorite group. Clay Miner. 25, 83–92.
Wolela, A., 2012. Diagenetic evolution and reservoir potential of the barremiane-cenomanian debre libanose sandstone, blue nile (abay) basin, Ethiopia. Cretac. Res. 36, 83–95.
Worden, R.H., Griffiths, J., Wooldridge, L.J., Utley, J.E.P., Armitage, P.J., 2020. Chlorite in sandstones. Earth Sci. Rev. 204, 1–38.
Xi, K., Cao, Y., Liu, K., Wu, S., Yuan, G., Zhu, R., Kashif, M., Zhao, Y., 2019a. Diagenesis of tight sandstone reservoirs in the upper triassic Yanchang formation, southwestern Ordos basin, China. Mar. Petrol. Geol. 99, 548–562.
Xi, K., Cao, Y., Liu, K., Wu, S., Yuan, G., Zhu, R., Zhao, Y., Hellevang, H., 2019b. Geochemical constraints on the origins of calcite cements and their impacts on reservoir heterogeneities: a case study on tight oil sandstones of the Upper Triassic Yanchang Formation, southwestern Ordos Basin, China. AAPG (Am. Assoc. Pet. Geol.) Bull. 103, 2447–2485.
Xiang, F., Wang, Y., Feng, Q., Zhang, D., Zhao, J., 2016. Further research on chlorite rims in sandstones: evidence from the Triassic Yanchang Formation in the Ordos basin, China. Arab. J. Geosci. 9, 507.
Yao, J., Wang, Q., Zhang, R., Li, S., 2011. Forming mechanism and their environmental implications of chlorite-coatings in Chang 6 sandstone (upper triassic) of hua-qing area, Ordos basin. Acta Sedimentol. Sin. 29, 72–79 (in Chinese with English abstract).
Yao, J., Zhao, Y., Liu, G., Li, Y., Luo, A., Zhang, X., 2018. Formation patterns of Chang 9 oil reservoir in triassic Yanchang formation, Ordos basin, NW China. Petrol. Explor. Dev. 45, 389–401.
Zhang, R., Hu, S., Zhang, X., 2017. Water-rock interactions and metal-alteration zoning in volcanic basins of Middle-Lower Yangtze River Valley. Acta Petrol. Sin. 3, 3302–3318 (in Chinese with English abstract).
Zhang, X., Lin, C., Cai, Y., Qu, C., Chen, Z., 2012. Pore-lining chlorite cements in lacustrine deltalc sandstones from the upper Triassic Yanchang Formation,Ordos basin China. J. Petrol. Geol. 35, 273–290.
Zhao, Z., Guo, Y., Wang, Y., Lin, D., 2012. Study progress in tectonic evolution and paleogeography of Ordos basin. Special Oil Gas Reservoirs 19, 15–20 (in Chinese with English abstract).
Zhou, D., Zhao, T., Zhao, P., Zhang, X., 2018a. Chlorite EPMA characteristic and its geological significance of the Kangshan Au-Ag-Pb-Zn deposit in west of Henan. Miner. Explor. 9, 803–824 (in Chinese with English abstract).
Zhou, X., Jiao, S., Yu, J., 2017. Occurrences and origin of chlorite films in the Yanchang formation sandstones, Ordos basin. Bull. China Soc. Mineral Petrol. Geochem. 36, 834–842 (in Chinese with English abstract).
Zhou, X., Wang, J., Lan, C., Dai, J., 2018b. Forming mechanisms of chlorite films in Yanchang formation, Ordos basin. Journal of China University of Petroleum (Edition of Natural Science) 40, 20–28 (in Chinese with English abstract).
Zhou, Y., Ji, Y., Xu, L., Che, S., Niu, X., Wan, L., Zhou, Y., Li, Z., You, Y., 2016. Controls on reservoir heterogeneity of tight sand oil reservoirs in Upper Triassic Yanchang Formation in Longdong Area, southwest Ordos Basin, China: implications for reservoir quality prediction and oil accumulation. Mar. Petrol. Geol. 78, 110–135.
Zhu, S., Wang, X., Qin, Y., Jia, Y., Zhu, X., Zhang, J., Hu, Y., 2017. Occurrence and origin of pore-lining chlorite and its effectiveness on preserving porosity in sandstone of the middle Yanchang Formation in the southwest Ordos Basin. Appl. Clay Sci. 148, 25–38.
Zhu, X., Deng, X., Liu, Z., Sun, B., Miu, J., Hui, X., 2013. Sedimentary characteristics and model of shallow braided delta in large-scale lacustrine: an example from Triassic Yanchang Formation in Ordos Basin. Earth Sci. Front. 20, 19–28 (in Chinese with English abstract).